UNIVERSITÀ DI GENOVA

SCUOLA DI SCIENZE MATEMATICHE, FISICHE E NATURALI

DIPARTIMENTO DI SCIENZE DELLA TERRA DELL'AMBIENTE E DELLA VITA

MASTER'S DEGREE IN HYDROGRAPHY AND OCEANOGRAPHY

Evaluation of Ground Control Points' displacement effects on photogrammetric accuracy using "Unmanned Photogrammetric Office" tool

Candidato:

Dinbayan Sarsenbay

Relatore:

Prof. Domenico Sguerso

Correlatori:

Dott. Sara Gagliolo
Dott. Ilaria Ferrando

Anno Accademico 2021-2022

Evaluation of Ground Control Points displacement effects on photogrammetric accuracy using "Unmanned Photogrammetric Office" tool

ABSTRACT

Nowadays, Unmanned Aerial Vehicle photogrammetry has already become an important application for extraction of Digital Surface Model (DSM), orthophoto, and other useful information of Earth surface in a comparatively short time. Technological improvement made it possible for UAV to offer numerous opportunities, including the generation of centimetric level accuracy mapping products. This can fill the gap between conventional airborne and very high-resolution satellite imagery in mapping and studying applications.

The aim of this study is to understand the influence of GCPs' configuration in the final accuracy of the related photogrammetric model, that was conducted by means of UAV. Due to the fact that placing and measuring GCPs on-field is the most time-consuming work, it is important to find out the configuration that will meet our expectations and will have good accuracy. Moreover, it is not always possible to place a GCP in the desired point due to accessibility or safety reasons. The accuracies of different configurations were evaluated using the simulation of the bundle block adjustment with a rigorous approach by comparing GCPs' number and distribution. The geographical coordinates of GCPs were measured using Total Station. Models were generated using "Agisoft Metashape Pro" software based on images captured using the "DJI Mavic Pro 2" drone from aligning the photos to the production of DSM and georeferenced orthophotos.

The quality of a final photogrammetric product is highly dependent on the flight planning of the survey. For this reason, a tool for planning a photogrammetric survey with UAV, called "Unmanned Photogrammetric Office" (U.Ph.O) was employed.

A single flight was conducted over a test field in Praglia village (Genoa, Liguria Region), involving the usage of 20 GCPs and 87 images in order to demonstrate how accuracy changes with different distributions of GCPs.

Valutazione degli effetti della dislocazione dei punti di appoggio sulla precisione fotogrammetrica attraverso il tool "Unmanned Photogrammetric Office"

SOMMARIO

Al giorno d'oggi, la fotogrammetria da UAV è già diventata un'applicazione importante per l'estrazione di Modello Digitale della Superficie (DSM), ortofoto e altre informazioni utili relative alla superficie terrestre in un tempo relativamente breve. Il miglioramento tecnologico ha permesso agli UAV (Veicoli Aerei senza Pilota) di offrire numerose opportunità nella mappatura, inclusa la generazione di prodotti di mappatura con precisione di livello centimetrico. Questo può colmare il divario tra le immagini aeree convenzionali e quelle satellitari ad altissima risoluzione nelle applicazioni di mappatura.

Lo scopo di questo studio è comprendere l'influenza della configurazione dei Ground Control Point (GCP) sull'accuratezza dei relativi modelli fotogrammetrici del rilievo, a partire da immagini ottenute tramite UAV. Poiché posizionare e misurare i GCP sul campo è il lavoro che richiede più tempo, è importante individuare la configurazione che soddisferà le aspettative e avrà una buona precisione. Inoltre, non sempre è possibile posizionare un GCP nel punto desiderato per motivi di accessibilità o sicurezza. La precisione delle diverse configurazioni è stata ottenuta mediante simulazione di rete con approccio rigoroso secondo il criterio di stima dei minimi quadrati ed è stata confrontata con il numero e la distribuzione dei punti di controllo a terra. Le coordinate geografiche dei GCP sono state misurate utilizzando la stazione totale. I modelli sono stati generati utilizzando il software "Agisoft Metashape Pro" sulla base di immagini acquisite utilizzando il drone "DJI Mavic Pro 2". Il software Metashape Pro è stato usato per tutte le fasi del post-processamento dall'allineamento delle immagini alla produzione di DSM e delle ortofoto georeferenziate.

La qualità di un prodotto fotogrammetrico finale dipende fortemente dalla pianificazione del volo UAV. Per questo motivo è stato scelto uno strumento per la progettazione di un rilievo fotogrammetrico con UAV, denominato “Unmanned Photogrammetric Office” (U.Ph.O).

Un singolo volo è stato condotto su un campo prova nella localita Praglia (Genova, Regione Liguria), prevedendo l'utilizzo di 20 GCP e 87 immagini al fine di dimostrare come l'accuratezza cambia con le diverse distribuzioni dei GCP.

INDEX

LIST OF FIGURES

LIST OF TABLES

LIST OF CHARTS

INTRODUCTION

Within past years, the use of Unmanned Aerial Vehicle (UAV) was persuaded by military objectives. Nowadays, UAVs evolved into widely used standard remote sensing platforms providing high-resolution geospatial data acquisition, that are used in surveying and mapping in a wide range of civil and commercial applications like agriculture, transportation, cultural heritage, archaeological surveys, environmental assessment, video and photo documentation, cadastral applications, etc. [14][10]

UAV is a vehicle that can be controlled remotely, semi-autonomously, autonomously, or even being a combination of these methods, while other measurement methods like close-range or aerial photogrammetry can be operated or be planned only manually or semi-autonomously. Huge advantage of UAV is that it can be applied in a survey of areas that could be dangerous to be carried out by humans, guaranteeing accuracy and precision of the survey. On the other hand, the limitations such as sensor quality, environmental conditions, weight, battery life, etc. may affect the performance of UAV. [6]

Advanced technologies allowed UAVs to work in a combination with Internal Motion Unit (IMU), navigation system, power unit, lightweight stereo camera, and other sensors. Since UAVs can be equipped with digital cameras, they can be also be involved in photogrammetric work. For photogrammetry, UAV platforms are used in geomatic applications to produce accurate 3D surface information thanks to recent advances in photogrammetry and computer technologies, which led them to become a feasible alternative to classical manned aircraft. This is possible due to the ability of these devices to provide high-resolution images of ground surface flying at low altitudes and having a comparatively lower cost of flight missions. [1][6][13][16]

The accuracy of a UAV survey is the result of different factors, particularly: flight design, image quality, processing software, quality of navigational systems, focal length, flight altitude chosen, camera orientation, Structure-from-Motion (SfM) algorithms, georeferencing methods, etc. It also has to be mentioned that UAV is dependent on external conditions of the field such as the texture of terrain, available lighting, and weather. Maintaining homogeneous coverage of the whole area and overlapping both transversally and longitudinally over the flight process, would be effective in post-processing of the images acquired. [2][3][5][7][8]

The technique called SfM (Structure-from-Motion), used in a number of modern photogrammetric software, automates the image matching task using high-precision mathematical algorithms. These algorithms search for key points through the analysis of the images generating sparse point clouds with bundle block adjustment (BBA). Then, the sparse point cloud is densified, at the same time eliminating gross errors, in order to get dense point cloud with the use of MultiView Stereo technique, that is paired with SfM tool. [1][2][15][16]

The SfM technique doesn't require total supervision of the operator, whereas the "Georeferencing" part of the survey stands in need of an operator's deep attention. The

reason to focus on this key part is that the point cloud created by the SfM technique is captured in the arbitrary frame and it has to be scaled and framed into a real-world coordinate system. Additionally, georeferencing markers are used also for camera calibration purposes. The georeferencing can be done in two ways: “direct” and “indirect”. In direct georeferencing, the transformation from arbitrary frame to the real-world coordinate system is achieved by using internal navigation sensors (GNSS, Global Navigation Satellite System and IMU, Internal Motion Unit). In theory, the direct measurement of coordinates is acquired at exactly the same moment of image capturing. However, this is quite a difficult task to perform taking into account that the velocity of a UAV can reach a value of over a meter per second. This is not the unique reason; it depends also on the type of GNSS solution (stand-alone or RTK, Real-Time Kinematic). On the contrary, indirect georeferencing requires the so-called “Ground Control Points” that are measured on the field by using a GNSS receiver or Total Station. Although direct georeferencing is carried out faster and cheaper, the accuracy will be less than indirect georeferencing even for high-resolution projects. The accuracy of direct georeferencing was proved to be higher because it reduces “the dome effect”, which is the systematic error caused by the correlation of inner and exterior orientation parameters, especially in nadiral images. [1][2][3][8][14]

The basic SfM workflow requires three GCPs to georeference the photogrammetric model using a Helmert transformation, but some modifications of the basic approach, such as those that allow coordinates to be included in the bundle adjustment, benefit from a larger number of GCPs. Indeed, it is recommended to use a significantly greater number of GCPs in order to increase the control on the final accuracy of the 3D model. [3][11]

These GCPs can be marked on the field before the survey or some artificial feature could be used as markers too. However, for high-precision end products it is suggested to place clearly visible markers on the field so they are easily detected on the acquired images as well even if this procedure is considered time-consuming. Manual selection method is used during the post-processing stage of the survey in order to detect the centers of each marker. [13]

The shape of the created 3D model will always adapt to the control points, and while the GCPs are used to generate photogrammetric output, the so-called Check Points (CP) are used to give the realistic assessment of the model’s accuracy, since CPs are not involved in photogrammetric modeling itself but only for evaluation of accuracy.

Another challenge with the GCP georeferencing technique is determining how accuracy changes according to their number and distribution because this is still an open issue.

Since the accuracy of the model is directly influenced by the accuracy of GCPs, their positions were obtained with Total Station in a local coordinate system. Due to the fact that this project is aimed to achieve higher accuracy values, the Unmanned Photogrammetric Office (U.Ph.O) software tool was applied. This tool uses the least-squares rigorous approach of network simulation taking into account terrain

morphology. Outputs of the U.Ph.O include realistic estimation of images overlapping and expected precision of the survey, which require some particular inputs such as flight height, overlap, the Internal Orientation (I.O.) parameters, the GCP coordinates, and a coarse DSM that represents the scene. [4]

The aim of this project is to understand the influence of GCP number and distribution on the accuracy of the final photogrammetric products evaluating the estimated accuracy of the project with the use of the U.Ph.O. tool. For this reason, the survey was conducted in the area of Praglia village (Genoa, Region Liguria) using a DJI Mavic Pro 2 drone to capture 87 images with uniformly distributed 20 control points. Then, the several tests have been conducted by changing the GCP configuration to state how the final accuracy of the photogrammetric model is affected.

In the first chapter of this project, the UAV will be introduced, mentioning its types, components, and legislative limits for operation. Then, the topic of UAV photogrammetry will be described in chapter two, mentioning the basics of photogrammetry, the process of photogrammetric mapping, the benefits and drawbacks of UAV photogrammetry, and its accuracy. The third chapter will include the U.Ph.O. project that was developed by Daniele Passoni during his Ph.D. thesis project. In the fourth chapter, the survey conducted in Praglia will demonstrate you the results obtained, then the actual accuracy will be compared with the predicted one. The conclusions are reported in the final chapter.

1. THE UNMANNED AERIAL VEHICLE (UAV)

A UAV, also known as a drone, is a flying machine that is operated remotely or in a mode not having any human onboard. Lately, the U.S. Department of Defense, followed by the European Aviation Safety Agency (EASA) approved the term UAS, which stands for "Unmanned Aerial System". This was done to demonstrate the importance of calling it "system" because it works as a combination of ground control stations, communication links, launch and retrieval systems, and the aircraft itself (which is now officially called "UAV"). Basically, these terms are mutually understood as a drone, though when it comes to regulatory issues the term UAS is considered official. [19]

Nowadays, there are many types of UAS, but previously manned aviation was developed in the 18th century in the form of heavy machines. Around the time of WW1, these heavy machines developed to become unmanned. Mentioning, for the first time it was demonstrated in 1916 by two inventors Hewitt and Sperry, which gained interest from U.S. Navy. However, this project was deprived of adequate accuracy and had many technical problems. [19]

Modern-day drones have a lot to offer, following the technical improvements, in such applications as scientific research (UAV photogrammetry), forest protection, search and rescue, aerial photo and video recording, traffic control tasks, infrastructure support, coastguard support, etc. [19]

Principle of working

Basically, drones are launched upwards with the help of sufficient upward force called "*Lift*", and are able to set in motion by the force called "*Thrust*". The lift is caused by low pressure at the top of the propeller or a wing and the high pressure under them. The lift depends on the inclination of a propeller. [21] The following figure represents how forces are distributed around the drone.

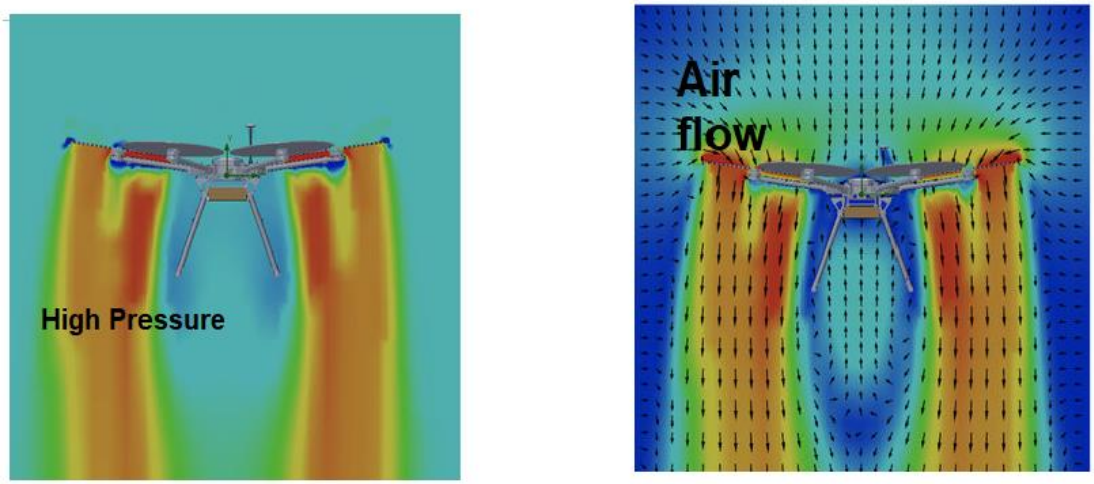

Figure 1-1: Total Pressure and Velocity contours respectively

Taking as an example regular multi-rotor or fixed-wing UAV, it has to be mentioned that there are four major forces acting on them: Weight, Lift, Drag, Thrust. Since multi-rotor UAVs do not have wings, they use propeller thrust force to generate lift force and to move through the air. Controlling the forces on top of each propeller, the aircraft can change its flight height, direction, and speed of flight. The fixed-wing UAV uses its wings to control airflow over its control surfaces. [21]

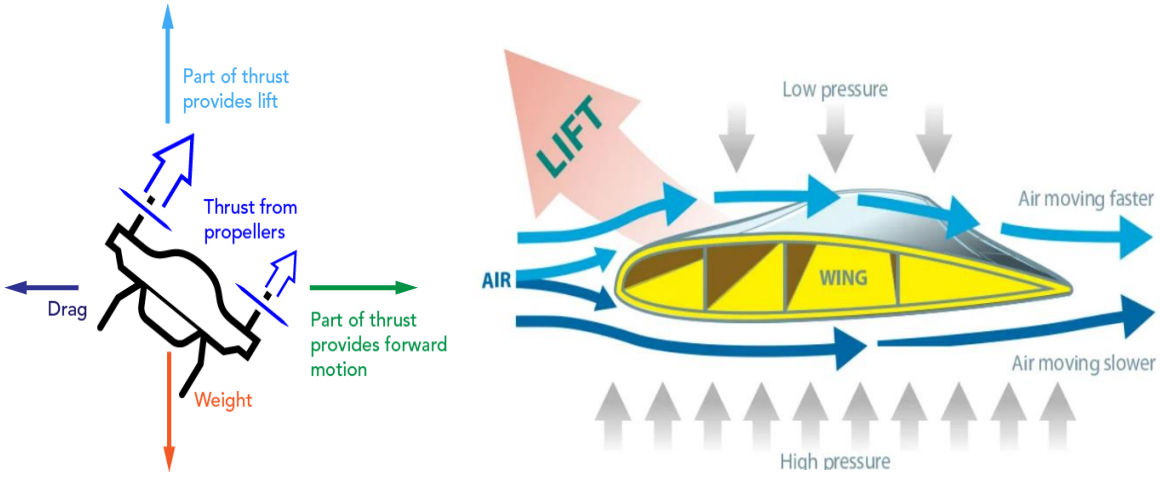

Figure 1-2: Forces acting on a rotary-wing (left) and fixed-wing (right) UAVs

UAV Classification

Aerial drone platforms nowadays have two main types: Rotary-Wing and Fixed-Wing

1) *Rotary-Wing*

Figure 1-3: Model of rotary-wing UAV

This type of drone is the most common due to its wide range of models being used in aerial photography. It has from 2 up to 16 rotary blades that turn around fixed masts distributed at equal distances from each other. As it was mentioned before, propellers are used to generate the “lift” force as their blades rotate through the air. [22][23]

Advantages	Disadvantages
can hover	short flight time (short battery life)
great maneuverability	reduced speed and load
vertical take-off anywhere	regular maintenance required
vertical landing anywhere	sensitive to weather conditions
cheapness	more dangerous than fixed-wing UAVs
	noisy
	unsuitable for large-scale aerial mapping

Table 1-1: Pros and Cons of working with rotary-wing UAVs

2) Fixed-Wing

Figure 1-4: Model of fixed-wing UAV

This type of UAV has a rigid wing like a normal airplane in order to generate lift, while thrust is generated by the engine. [22][23]

Advantages	Disadvantages
high endurance (can be powered by the gas engine)	impossible to hove
lighter than rotary-wing drones	impossible to vertically take-off
less dangerous	impossible to vertically land
less complicated	comparatively expensive
comparatively silent	training required
heavier loads	runway, net, or parachute is needed to land
can fly at high altitudes	
more stable in the air	

Table 1-2: Pros and Cons of working with fixed-wing UAVs

Moreover, UAV types described hereabove can be further categorized based on their size, weight, endurance, flying height, etc. These parameters must be considered before launching because each State has its own regulations regarding the use of drones. One of the main goals of drone operations is to conduct everything in a safe mode. So, parameters like the maximum weight of the drone have to be calculated. This is important because the weight directly influences the kinetic energy applied. Obviously, this value is much higher in populated areas or even can be prohibited at all. However, some mini versions of drones exist that are almost impossible to cause any danger to people and aviation as well, due to their low altitude of operations. Another example of safety consideration is the classification of UAVs by their altitude of operations in order to dictate collision avoidance requirements. [19]

UAV components

UAVs are complex technologies comprised of software and hardware components. A UAV key parts may be classified into three groups: the platform itself (UAV), the ground control station (GCS), and the communication system. [24]

The aerial platform is made up of many parts whose roles are to allow the platform to fly and store required data-gathering sensors onboard. The main of them is the airframe, which is the structure of the UAV. The airframe has to be withstanding external forces that can occur during the flight not causing any deformation and/or vibration. Its structure has to consider the weight regarding the power, the communication, and the control systems. Fixed-wing drones are commonly expected to be made of polystyrene or plastic, while rotary-wing drones are made of aluminum or carbon fiber making them light and resistant. [24]

The navigation system is made up of a flight controller, GNSS receiver, and IMU. The flight controller is in charge of flight planning and may compare the theoretical and actual paths. It is possible to connect many sensors to this board and synchronize data collecting using GPS time. In certain cases, it is possible to insert a card in order to retain additional data such as a log file, telemetry, images, or other files. The GNSS receiver used onboard UAV is a single-frequency and dual constellation system (GPS/GLONASS). The IMU system is also an important part of the navigation system, which is mounted onboard to regulate the attitude of the UAV. The drawback of this system is that it cannot store raw data, while the precision for mini-UAVs lately was estimated for around 1-4 degrees. The IMU is comprised of a set of accelerometers and gyroscopes that are required to assess all of the navigation variables at a high rate. Since they are electromechanical sensors, systematic mistakes such as measurement bias, scaling factors, and inadvertent errors caused by noise can all impact the results. Another essential element of the UAV is the power system, which is responsible for supplying energy to the system. Different power systems can be used depending on the chosen airframe: rotary engines, fuel cells, electric solutions, and even lithium polymer batteries that were later adopted in rotary-wing drones. [24]

The payload is made up of sensors that are carried by the UAV to collect data or some other parameters such as camera, thermal sensor, etc. Instruments for onboard equipment and gadget activation might be among the payload's other components. A gimbal, which allows the payload to rotate along several axes and is generally fitted with actuators to change or stabilize the sensor's orientation, is a critical component, particularly in the case of cameras. The gimbal may be fixed, stabilized, and operated from the ground using the sensors. [24]
The ground control station (GCS) provides continuous and interactive remote control of the UAV while also updating the operator on the autonomous flight's status. The fundamental setup for a GCS is generally a computer or a tablet that can plan and control the flight. If the UAV is not totally autonomous, the pilot should have a remote control that may be utilized in an emergency or to execute takeoff and landing. Commercial UAVs have their own specialized mission planners, or open-source software produced by the scientific community can be used. Mission planners are programs that allow you to plan a photogrammetric flight or construct a sequence of navigation waypoints by specifying the area of interest, camera specifications, and other photogrammetric variables (e.g., overlapping, ground sampling distance, etc.).
The communication system, which is the radio link between the ground station and the aircraft, is the last UAV component. Radio communication is required to instruct and operate a UAV, as well as to ensure continuous connectivity for emergency operations. [24]

Regulations on UAV

Nowadays, the use of UAVs gained interest not only for specialized applications but also among civilians for flying-for-fun practice. In order to maintain aerial space safe for people and aircraft, the need for implementation of regulations was raised.
The first example is related to the Australian Civil Aviation Safety Authority (CASA) in 2002. The document, mentioning the requirements to obtain the certification of drone operators, had to guarantee both proper theoretical and practical education. In the European Union (EU), the European Aviation Safety Agency (EASA) is responsible for the arrangement of legislative measures for civil use of UAVs with a Maximum Take-Off Weight (MTOW) of more than 150 kg. UAVs with a MTOW of less than 150 kg. fall under National Aviation Authorities. In some European countries, the UAV regulations have already been entered into force - Italy is one of them. [4]
ENAC (Ente Nazionale per l'Aviazione Civile) – the national agency for civil aviation is an Italian regulatory organ responsible for the use of UAVs in the airspace of Italy. The main objective of the ENAC is to maintain the high-level safety of UAV operations eliminating the risks, taking into account conditions of weather, population density in the operation area, MTOW, speed of the drone, communication means, and more. Depending on the level of associated risk, ENAC introduced three categories of drone activities: [25]

Open category: given the low level of risk involved, the necessity of approval from competent authorities is considered negligible. Additionally, no self-declaration from a drone operator is required. The "*open*" category of UAV operations is divided into three sub-categories according to the regulations. The operations have to be recognized as UAV operations in the "*open*" category only when the following parameters are completed:

- MTOW is less than 25 kilograms
- the operator keeps the drone at a safe distance from people and it is not flown over a crowd of people
- the UAV has to be kept in visual line of sight (VLOS) except for the situations when the operator is flying in follow-me mode
- a maximum altitude of 120 meters above the ground level must be kept always, except when avoiding an obstacle
- during the flight the drone must not have any dangerous goods on board

Specific category: given the moderate level of risk involved, it is required to have a flight approval from competent authorities prior to operation. Except for particular cases where an operator declaration is sufficient, approval is given based on mitigation measures outlined in an operational risk assessment.

Certified category: Given the high level of risk involved, the drone must be certified and a remote pilot must be licensed. The operation falls under this category if the operation is conducted over assemblies of people, involves the transportation of people, and/or involves the carriage of dangerous goods. [25]

OPERATION		UAS			UAS OPERATOR	REMOTE PILOT	
Sub-category	Operating Area	Class	Mass/Impact energy/Speed	Operating Date Limitations	Registration	Min. Age (solo flight)	Competency
All	• Max height 120m/400ft (See UAS.OPEN.010 [3] & [4] for spesific obstacle and sailplane limits) • No dropping of articles • No carriage of dangerous goods					If directly supervising another remote pilot - 16	
A1	• May fly over uninvolved people, however, this should be avoided whenever possible, and where it is unavoidable, extreme caution should be used • No flight over crowds	Privately built	<250g & <19m/s	Nil	Only if 'camera' equipped (but not toys)	Nil	Read user manual
		Legacy (placed on market before 1 Jan 23	<250g			16 (unless reduced in State)	
		C0 (toy)	<250g & <19m/s			Nil	
		C0 (not a toy)				16 (unless reduced in State)	
	No intentional flight over uninvolved persons	C1	<900g & <80J	Nil	Yes	16 (unless reduced in State)	• User manual • Online training • Basic online exam (unless defined differently in State)
		A1 transitional (Article 22)	<500g	Not after 1 Jan 23			
A2	No closer than 30m horizontally from uninvolved persons (5m in 'low speed' mode 3m/s)	C2 (can also be used in A3)	<4kg	Nil	Yes	16 (unless reduced in State)	• User manual • Online training • Basic online exam • Self-practical training • A2 Theoretical Test
	No closer than 50m horizontally from uninvolved persons	A2 transitional (Article 22)	<2kg	Not after 1 Jan 23			
A3	• No uninvolved people present within the area of flight • No flight within 150m horizontally of residential, commercial, industrial or recreational areas	C3	<25kg	Nil	Yes	16 (unless reduced in State)	• User manual • Online training • Basic online exam
		C4					
		Privately built					
		Legacy (placed on market before 1 Jan 23)					
		A3 transitional (Article 22)	>2kg to <25kg	Not after 1 Jan 23			

Table 1-3: EASA Summary Table of Drone Flight Operation Requirements (https://www.easa.europa.eu)

2. THE UAV PHOTOGRAMMETRY

Photogrammetric basics

Photogrammetry is the technique of creating accurate two-dimensional or three-dimensional maps using images as a fundamental medium to perform precise measurements. Photogrammetry can be aerial or terrestrial. Terrestrial photogrammetry uses images taken from the ground, whereas aerial photogrammetry uses images taken from aerial vehicles above the ground. Aerial imagery can be taken in a nadiral or oblique mode. Nadiral images are those where the plane of the images is parallel to the ground.

The whole procedure beginning from acquiring the photos through processing them and up to using them either for interpretation or further computation and analysis is called photogrammetric processing.

To begin with, it is important to understand how the images differ from a map. The map is the cartographic material that can be used for making measurements. Since it has an orthographic projection, each object will have exactly the same location both in reality and on the map. The image, instead, sees through the lens, which is a sensor, in the center of the projection and puts everything into perspective. In the processing part, we convert perspective projection into orthographic one to make a reliable map out of the images. Two things need to be addressed when we talk about the processing of images: perspective and relief distortion. If we take into account the datum plane and the relief, we can sometimes see how differently it will be depicted on the photo because of the projection. We want our orthophoto map to be cartographic so the object will have exactly the same location on the ground and on the image and be eligible for quantitative measurements. This is obtained by means of orthorectification. Orthorectification is the process that removes the geometric perspective, effects of relief displacement, and optical distortions from the sensor. The resulting image is called an orthophoto or orthoimage. Final products have geometric precision of the orthophoto map, so can be treated as a map. It is possible to add a grid and a scale to an orthophoto, as well as to orient it, which would not be possible if the projection was not modified. [32]

Orthorectification was analogous in old times when huge machines were used to match photos by means of stereo pairs. Nowadays, it is done digitally by utilizing photogrammetric software. The principle of shifting perspective is the same in both analog and digital orthorectification techniques. [32]

In order to create an orthophoto we need:

- DSM to remove the relief distortion
- External orientation parameters (estimated from raw images) from aerial triangulation
- Camera calibration report (estimated from raw images) to transform perspective to ortho projection
- Ground Control Points for georeferencing and to reduce distortions

- Photogrammetric processing software that utilizes collinearity equations

Digital imagery

Geotagging an image is associating a picture with the geographical location (latitude, longitude, altitude). In theory, every part of an image can be tied to a geographic location, but in the most typical applications, only the position of the sensor is associated with an entire digital image. However, when it comes to fine-scale with the UAV imagery, it is important to have an exact location of every single point on the photo. [32]

GPS in the camera of UAV measures the location with very low accuracy. This is due to the fact that it is in the air when the shutter triggers only for a fraction of seconds, so it is not enough time to estimate the exact location. [32]

SfM is the range imaging technique that comes from computer vision concepts, and it estimates 3D structures from overlapping 2D image sequences. SfM identifies distinguishable points that can be recognized on the other pictures, resulting in many tie points. Throughout the whole photogrammetric process, it is important to remember the purpose of the project and for what the data will be used. The first phase is flight planning. [32]

Survey planning

The first thing to do before conducting the survey is to consider certain parameters. Questions listed below are some of the many factors to be considered:

- What final data is needed?
- What is an area of interest?
- What type of UAV platforms are required and what are their capabilities?
- What kind of sensors are needed for the purpose of the survey?
- What is the cost, labor, and time consumption assumption?
- Is it legal to fly there? Are there any permissions to be obtained?
- Is the area accessible? Are there any obstructions to be considered beforehand?
- What coordinate system shall be used for the survey?
- What is the weather outside for the required period of time?

etc.

Flight planning itself is a multistep procedure that includes flight planning, site evaluation, and flight control stages.

1) Flight planning

It starts with mission area assessment checking whether it is easy to access the destination by car or walking and get UAS to the field. Next is the planning of geometric parameters, which is bound with what the planning software requires to input in order to proceed with the next steps, which include choosing flight planning and flight logging platform with its further creation (sometimes manufacturer software is available or it is possible to use the one in free access). Next important thing is to assess the weather conditions in advance.

Based on parameters such as desired overlap, the size and elevation of an area to be surveyed, focal length of the camera to be used, the speed of the aircraft, the mission planner of a drone calculates the flying height, the location of the photogrammetric block, time interval between exposures, and the total number of images required.

2) *GCPs. Reference frame*

Geotagging is assigning the position of the sensor of the camera on the ground. The problem is that the position of a point on the photograph is not the same as the position of a point on the real Earth's surface. Therefore, an accurate position is achieved by using GCPs. GCPs can be either any feature on the ground that is easily distinguishable, unmovable, and not covered by vegetation, and they can be surveyed before/after the flight. We used pre-marked panels with the cross in the center to make them easily recognizable in the images. We use GCPs because we want to orient the image not only relative to each other but also to know their absolute location in relation to the datum. GCPs improve the precision of the model because the accuracy of the measuring GPS or Total Station is much better than the accuracy of the GPS on the UAV. [32]

GCP survey is an essential step in flight planning. Here, it is advised to have a minimum of 3 GCPs with recommendations to use more in cases of complex topography. Before measuring GCPs coordinates, the coordinate system, GCP accuracy, and topographic equipment needed must be defined.

3*) Site characteristics evaluation*

The next step in flight planning is the terrain check: looking around for high obstacles and features unsuitable for flight in the locations of take-off, mission, landing, and alternative landing. Here, alternative landing is meant by a location that would serve as an emergency area in case the first landing location will become inaccessible.

As soon as arriving on site, it is necessary to assess the weather and compare it with the predictions, because the temperature in the air may significantly influence the battery life. Moreover, some types of drones are just unable to operate under certain weather conditions like rain and snow. Also, shadows from clouds can obscure a lot of details on the field, therefore, it is advised to work under conditions of cloud coverage of less than 10%. Another important factor to mention is the time of the day during shooting, because the sun's illumination, affects both the quantity of reflected light to the aerial camera and its spectral quality. Moreover, there is a risk of hotspots appearing bleaching out portions of images. [18]

The personnel involved in the operation has to be distributed across the area for keeping visual contact with the drone during the flight and also advising people to stay at a safe distance. [32]

4) Flight control

The UAV pilot in command should launch, operate, and recover the drone from preset locations so that the aircraft will fly according to the mission plan. After UAV is launched, the crew should have a clear view of the aircraft at all times. To ensure the flight is going according to the flight plan, the pilot and visual observers must be able

to maintain effective communication with each other at all times. Upon any failure or any loss of visual contact with the UAV, the pilot should command the aircraft back to recovery position or utilize the built-in fail-safe option to recover the aircraft. [32]

Photogrammetric processing

Photogrammetric approaches function by simulating the image acquisition process and re-projecting each pixel to its correct place, enabling very precise measurement correcting all the distortions (due to camera tilt, scale, surface relief, etc.). Because vertical images have fewer distortions, it is possible to extract two-dimensional measurements from an image if the scale is known. However, the Earth surface is almost never perfectly even surface, for this reason, it is required to work in 3D to have accurate results.

The main principle of 3D measurement in photogrammetry is triangulation. During capturing at least two photographs from different positions, the "rays" can be created from each camera to point to the object. One "ray" is electromagnetic energy reflected from an object. Three-dimensional coordinates of the point of interest are obtained by the intersection of these "rays". Knowing the internal and external orientation parameters of the camera, the image measurements are converted into "rays" in order to perform photogrammetric triangulation.

I.O. parameters model the geometry inside the camera (focal length, origin, lens distortion), matching positions on the image with the associated coordinate system of the camera. I.O. parameters can be obtained by camera calibration or estimation in bundle block adjustment.

E.O. parameters adjust the position and rotation of the image at the moment of shooting with respect to the ground coordinate system. In total, E.O. is described by six independent parameters. The camera orientation is usually described by angular and rotational parameters: omega, phi, and kappa for roll, pitch, and yaw respectively. [26]

With the help of georeferencing, 2D image coordinates can be projected to the 3D coordinate reference system used for mapping.

Since the exposure station (lens nodal point) of an image, a point on the ground coordinate system, and a photographic image lie on the same straight line despite the presence of tilt of an image, the representation of the alignment between them can mathematically be described by collinearity equations. [26][29]

$$\xi = \xi_0 - c * \frac{r_{11}(X - X_0) + r_{21}(Y - Y_0) - r_{31}(Z - Z_0)}{r_{13}(X - X_0) + r_{23}(Y - Y_0) - r_{33}(Z - Z_0)}$$

$$\eta = \eta_0 - c * \frac{r_{12}(X - X_0) + r_{22}(Y - Y_0) - r_{32}(Z - Z_0)}{r_{13}(X - X_0) + r_{23}(Y - Y_0) - r_{33}(Z - Z_0)}$$

where:

ξ, η = measured coordinates

ξ_0, η_0 = principal point coordinates
c = principal distance
r_{ij} = nine direction cosines expressing the angular orientation
X,Y,Z = ground point coordinates
X_0, Y_0, Z_0 = exposure station coordinates

A least-squares adjustment is used to estimate the unknown parameters since there are typically more redundant measurements yielding more equations than there are unknowns in the equation. [29]
So, in order to create accurate 3D structure in software, we need photogrammetric software that utilizes collinearity equations. In our case, Agisoft Metashape Pro software was used.
Agisoft Metashape Professional is an image-based solution aimed at creating 3D content from still images.
Processing workflow includes three stages:

1) Pre-processing

It comprises image uploads in software as well as the loading of camera positions from the flight log. If the external parameters are in the EXIF file (as they are in DJI), the images will load automatically. [31][32]

2) Processing

Aligning photos

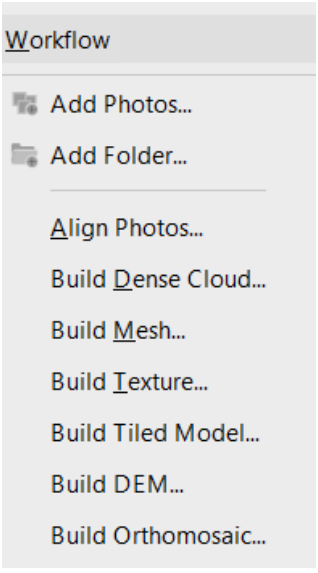

At this point, Agisoft Metashape uses SfM algorithms to track the movement of features across numerous images in a series. It obtains the relative position of the acquisition positions and refines camera calibration parameters so it is possible to see interior orientations of the camera calibration report. As a result, a sparse point cloud and a set of camera positions are generated. So, each photo is taken in the so-called Bundle Block Adjustment (BBA), which is a non-linear method for refining SfM and minimizing reprojection error. This way, it defects various geometrical similarities such as object edges or other specific details, subsequently monitoring the movement of those points throughout the sequence of multiple images. Using this information as input, the locations of these feature points can be estimated and rendered as a sparse 3D point cloud.
We have several accuracy settings to choose from photos alignment - usually high and low. While high accuracy alignment setting requires more time and memory space resulting in more accurate camera position estimates, the low accuracy setting renders rough camera positions. [31][32]

Building dense point cloud

At this stage, Agisoft Metashape calculates depth maps for every image. It also has several quality options to choose from: the higher the quality the more accurate camera position estimates are obtained but the process is more time-consuming. There are also different depth filtering modes, algorithms sorting outliers, which can appear due to some factors like poor texture of some elements of the scene, noisy or badly focused images:

- Mild depth filtering mode:

used for complex geometry where important features are not to be sorted out.

- Aggressive depth filtering mode:

sorts out most of the outliers, resulting in a smooth model.

- Moderate depth filtering mode:

gives results between mild and aggressive modes.

The resulting product is the dense point cloud. [31][32]

Building mesh

This step is necessary for building a 3D continuous model. Mesh connects points created during dense point cloud generation, creating so-called faces that are in form of triangles. There are two mode choices of mesh:

- Arbitrary:

it may be used to model any kind of element. On one hand, it can be selected for closed objects such as statues and buildings, on the other hand, it has high memory space consumption.

- High field:

it is used for modeling planar surfaces. Moreover, could be used for aerial photography. The advantage of high field is that it has low memory consumption compared with arbitrary mode. This is achieved by not taking into account spots underneath the objects. It is also called 2.5D mesh.

The source for the mesh generation could be a sparse cloud or dense cloud. Although sparse cloud generates 3D model faster, it results in its low quality. For the reason that the dense cloud gives higher quality output based on the previously reconstructed dense point cloud, it becomes an apparent choice of source data. [31][32]

Additionally, building mesh can be edited by several tools in order to get better quality output data. For example, the Close Holes tool repairs a 3D model if the reconstruction procedure resulted in a mesh with several holes, due to insufficient image overlap.

Generating texture

After building mesh, it is necessary to give color to each face generated. Several options are available through the texture mapping modes:

- Generic

it creates as uniform texture as possible.

- Adaptive orthophoto

it divides the object surface into two parts: the flat part and the vertical region. The orthographic projection is used to texture the flat part of the surface, whereas vertical

parts are textured individually to ensure proper texture representation. Adaptive orthophoto has a more compact texture representation for nearly planar scenes and good texture quality for vertical surfaces.

- Orthophoto

the whole object surface is textured in the orthographic projection. As a result, even more, compact texture representation than the Adaptive orthophoto at the expense of texture quality in vertical regions.

- Spherical

used only for ball-shaped objects.

- Single photo

gives texture from a single photo.

- Keep UV

generates texture, rebuilding the current texture with different resolutions.

Generating DSM

In order to generate the DSM, firstly, it is necessary to choose the source data in parameters, and also whether it is better to enable or disable interpolation. Disabled interpolation produces accurate reconstruction results because only areas corresponding to dense point cloud points are reconstructed, whereas enabling interpolation causes Agisoft Metashape Professional software to calculate DSM for all regions of the scene that are recognizable on at least one photograph. [31][32]

Generating Orthophoto

The last stage of processing workflow is orthophoto generation, which also needs a surface to use. Here, DSM is suggested that was generated in the previous stage rather than mesh. After choosing a surface, it is necessary to choose blending mode:

- Mosaic

implements an approach with data division into several frequency domains which are blended independently.

- Average

uses the weighted average value of all pixels from individual photos.

- Disabled

the color value for the pixel is taken from the photo with the camera view being almost along the normal to the reconstructed surface at that point.

3) Exporting results

Agisoft Metashape Professional software supports different options of
exporting results such as point cloud, mesh, DSM, orthophoto, after completion of the corresponding processing stage. Another useful option is the export of the Processing report. Its generation gives orthophoto and DSM sketches, camera parameters and survey schemes, tie points data export, image overlap statistics, camera positioning error estimates, and ground control point error estimates. [31][32]

3. THE UNMANNED PHOTOGRAMMETRIC OFFICE

Photogrammetric survey precision

Understanding photogrammetric survey metric capabilities entail not only recognizing its ability to generate a numeric reconstruction of the observed objects, but rather its ability to assess its precision, both a priori and a posteriori. Knowing the a-posteriori precisions involves validating the survey and indicating the quality and applicability boundaries of the data. Prior to knowing the achievable precisions, it is required to plan the survey and the circumstances that will ensure the survey precisions are reached.

It is helpful to start with Fraser's paper "Network design considerations for non-topographic photogrammetry" to better understand the idea of precision evaluation. According to the author, accuracy is impacted by the geometry of the network, or "network design", as well as the quality of the observations (measurement of the coordinates of the points on the images). Fraser has followed Grafarend's classification scheme to identify problems of network design:

1) Zero-Order Design (ZOD)

The Datum problem involves the choice of an optimal reference system for the object space coordinates.

The datum problem is indeed solved by the introduction of the coordinates of some control points, whose number is equal or greater than the rank deficiency to fix the reference system. The minimum request is satisfied by 2 control points with all 3D information (XC, YC, ZC) and one control point in height (ZC) opportunely located.

2) First-Order Design (FOD)

The Configuration problem is concerned with the search for an optimal network geometry for a given array of object target points.

FOD problem, at least for the normal case, is mainly influenced by the base-to-distance ratio (B/D), i.e., the ratio of the distance between two consecutive overlapping images and their distance from the object, because a decrease in the B/D ratio leads to a less favorable ray intersection geometry. Several other parameters affect the camera network strength, like the number of camera stations, the number and multiplicity of tie points, the image scale, the sensor size, and the focal length.

3) Second-Order Design (SOD)

The Weight problem involves the search for an optimal distribution of observation work.

4) Third-Order Design (TOD)

The Densification problem concerns the question of how best to enhance the precision of a network through the addition of extra object points and observations.

As previously stated, the available literature provides beginning points for further investigation of the ZOD. The issues of TOD and SOD, on the other hand, have less of an impact on the FOD. As a result, it's critical to go further into the configuration problem and give effective planning tools. [4]

The estimation of precision by Krauss

Using the stereo restitution method, Krauss offers an assessment of predicted accuracies assuming that the camera planes are parallel and normal to the base connecting the cameras. In aerial photogrammetry flights, when cameras are housed on stabilized platforms, this requirement is almost usually satisfied; nevertheless, if deviations from ideal circumstances (e.g., camera axis off-nadir larger than 5°) are too significant, the mission must be repeated. Thus, the object coordinates may be computed from the quantities observed on the picture, and the accuracy of these indirectly obtained coordinates can be assessed. Among accuracies of coordinates listed below, the analyzed standard deviation is more significant along Z-axis.

$$\sigma_x = \sqrt{(\frac{\xi}{c}\sigma_z)^2 + (m_b\sigma_\xi)^2}$$

$$\sigma_y = \sqrt{(\frac{\eta}{c}\sigma_z)^2 + (m_b\sigma_\eta)^2}$$

$$\sigma_z = (m_b\frac{h}{B}\sigma_{p_x})$$

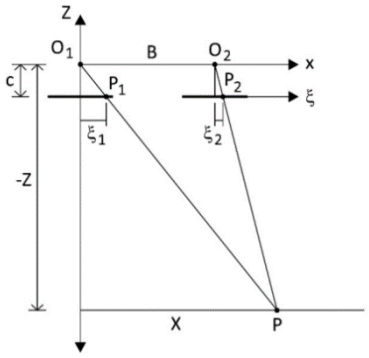

The accuracy of the elevation is as follows, assuming the principal distance c and base B are both error-free:

$\sigma_Z = \frac{Z^2}{cB}\sigma_{\rho\xi}$, where Z is the relative height and $\sigma_{\rho\xi}$ is the precision of the measurements on the images.

However, the most practical and economical method of producing cartography was stereo restitution, it eliminates the potential of convergent imaging and the visibility of an object point in more than two images. The methods of the photogrammetric shooting have evolved significantly as a result of the use of digital cameras, unmanned aerial vehicles, and technologies generated from computer vision, leading to the cases where typical stereo requirements are practically never matched. [4]

The estimation of precision by Fraser

Because of the large percentage of overlap and the existence of oblique photographs, the correlations utilized for terrestrial close-range photogrammetry vary dramatically. In reality, the number of images and their convergence are critical factors to consider when establishing the final accuracy.

According to Fraser, the precision of an object coordinates is expressed as:

$$\sigma_{XYZ} = \frac{qZ}{c\sqrt{k}}\sigma_{\rho\xi}$$

where Z is the distance between the object and the camera, c is the focal length, k is the number of overlapping images, q is a form factor and $\sigma_{\rho\xi}$ is the precision of the measurements on the images. The latter component is highly dependent on the measuring method employed and the image quality. It can be presumed to be proportional to the pixel size in calibrated non-metric cameras. The model of accuracy adapts better to the conditions of a photogrammetric survey by UAV thanks to the addition of the parameters k and q, which take into account the large overlap of photographs and the shot geometry, which commonly proves to be convergent. Whereas the number of overlapping photographs k is a parameter that can be easily defined, the form factor q is a parameter that can only be calculated by empirical examination of numerous datasets from UAV surveys. According to Fraser, the form coefficient q may be derived to be 3.5 in the case of nadiral acquisition with a typical overlapping of 60% of the picture size. When there is a lot of cross overlapping, it drops to 3 and when there is a lot of convergent geometry, it drops to 0.4. [4]

The rigorous approach

It becomes apparent that the described methods of a priori estimation techniques of predicted precision appear to be unreliable in many cases. The reason for this is that Krauss' technique ignores the redundancy of tie point observation and simplifies the imaging geometry, whereas Fraser's method necessitates the knowledge of a factor q that is difficult to estimate in complicated imaging geometry. Since the UAV survey is considered a complicated imaging geometry process, a more rigorous method is needed.

Unfortunately, both the approaches described above are focused on the variance propagation of photogrammetric restitution, which ignores the uncertainties arising from the process of photogrammetric block orientation. However, if it is necessary to obtain a precise estimate of the predicted precisions, we must return to the problem's general formulation via Bundle adjustment. Here, the triangulation approach is used to rebuild a points cloud characterizing an object or an area, with image coordinates being the fundamental observables.

The linear functional and stochastic model may be stated as follows:

$v = Ax - 1$

$C_{II} = \sigma_0^2 * P^{-1}$

where l, v, and x are the vectors of observations, residuals, and unknown parameters, respectively; A is the design matrix; C_{II} is the covariance matrix of observations; P is the weight matrix and σ_0 is the variance factor.

From the least-squares theory, the covariance matrix of the unknown parameters C_{xx} can be written as:

$C_{xx} = \sigma_0^2 (A^T P A)^{-1}$

For the (X, Y, Z) coordinates of the object points, the trace of the C_{xx} matrix provides the variance and, as a result, the precision. We may simulate this network and get the standard deviation for each point inside the survey area using an approximate DTM

(at least 5 meters of resolution), Internal Orientation (IO) of the camera, and the External Orientation (EO) of planning, given that it is visible on at least a couple of images. The precision of the measurements on the pictures ($\sigma_{\rho\xi}$) is set to one pixel, and the a posteriori σ_0 is set to 1/3 of the ground pixel size in this case (GSD). [4]

The Aim of the U.Ph.O. project

The challenge of a priori evaluation of achievable precisions is neglected by all available software. U.Ph.O. was developed in MATLAB with the goal of offering flight planning tools that take into account the needed metric precisions while also providing a priori information on predicted precisions, Ground Sample Distance, and number of observations (number of collinearity rays per object point). The created tool is divided into two sections: Analysis and Plan. [4]

The Planning

The planning component allows a photogrammetric survey by UAV to be planned. It generates flight settings that are required to plan an autonomous mission for navigation software. Knowing the precisions that can be achieved across an object surface could be highly important in modifying the original survey plan, particularly in terms of metric quality.

As already mentioned, the rigorous method of precision evaluation is the best choice to achieve high accuracy results. On the other hand, an excessive approach could cause collision dangers, increase time consumption, etc. In fact, it's crucial to understand that a tool for obtaining realistic planning for a UAV survey could be useful in situations where it's critical to assess the proper balance between expected accuracy and distance from the object in order to navigate safely and efficiently.

U.Ph.O., firstly, requires some parameters to be inserted beforehand, including:

- Shooting geometry of the camera
- Relative flight height and/or GSD
- Overlapping of images along the route
- Coarse DSM

The workflow begins with the input of limits of the project: I.O. parameters (focal distance, principal point, sensor format size) of the camera followed by the selection of an area of interest with a Graphical User Interface as a background layer, the overlapping of images (both transversal and longitudinal), shooting geometry, strips directions, and flight altitude. Once set up, projection center positions and altitudes of all images are defined.

Upon specifying the flight parameters, the program suggests checking if the survey accuracy criteria are satisfying. For this reason, it is necessary to upload a DSM. Along with DSM, the take-off coordinates are required in order to obtain effective overlapping of images, realistic visibility, and occurrence maps. Visibility and occurrence maps are created in U.Ph.O. by using collinearity principles examining which DSM cells appear in each image projection center. As a result, an “overlap”

map is produced which can be exported in GeoTiff format and can then be opened in GIS software.

The final step includes using the rigorous technique established in U.Ph.O. to estimate the predicted precisions, treating each DSM cell separately. It is required to determine the number and position of GCPs that will be measured on the ground at the time of the flight in order to estimate precisions using the rigorous approach.

From the matching occurrence map pixel and the survey parameters, a block design matrix "A" is produced for each cell (position and attitude of every camera). A is an m×3 matrix, where m is equal to twice the times the cell is seen in the images. By inverting the normal matrix N, the covariance matrix Cxx is constructed, which provides the planimetric and altimetric standard deviations of each DSM cell.

If the expected precisions do not meet the project objectives, the overlapping is insufficient, or too many points fall into obstructed areas, the planning parameters can be changed (flight altitude, overlap percentage, number and position of GCPs) and the project can be run again.

The Analysis

Since any survey may go wrong due to environmental conditions, instrument failure, or any other reason, U.Ph.O. features a module that reviews an already completed survey. If it seems that any factor has adversely affected the quality of a survey, it is necessary to re-analyze obtained data before the processing stage. Then, if necessary, the flight can be performed again.

4. THE CASE STUDY

Study area

The realistic planning has been applied as a simulation to a survey conducted on 5th of August 2021, represented by an area of around 500 m^2 located near Praglia (Liguria, Italy). The area was chosen far from the urban zone to avoid external interferences, because the survey was meant to be conducted by means of UAV (DJI Mavic 2 Pro). The utilized DJI Mavic 2 Pro platform was equipped with 20 megapixel 1'' CMOS sensor. Total Station (Leica T-CR 703) was used for the purpose of referencing Ground Control Points. 20 square markers of yellow and black colour were spread across a survey area to serve later as control points and/or check points.

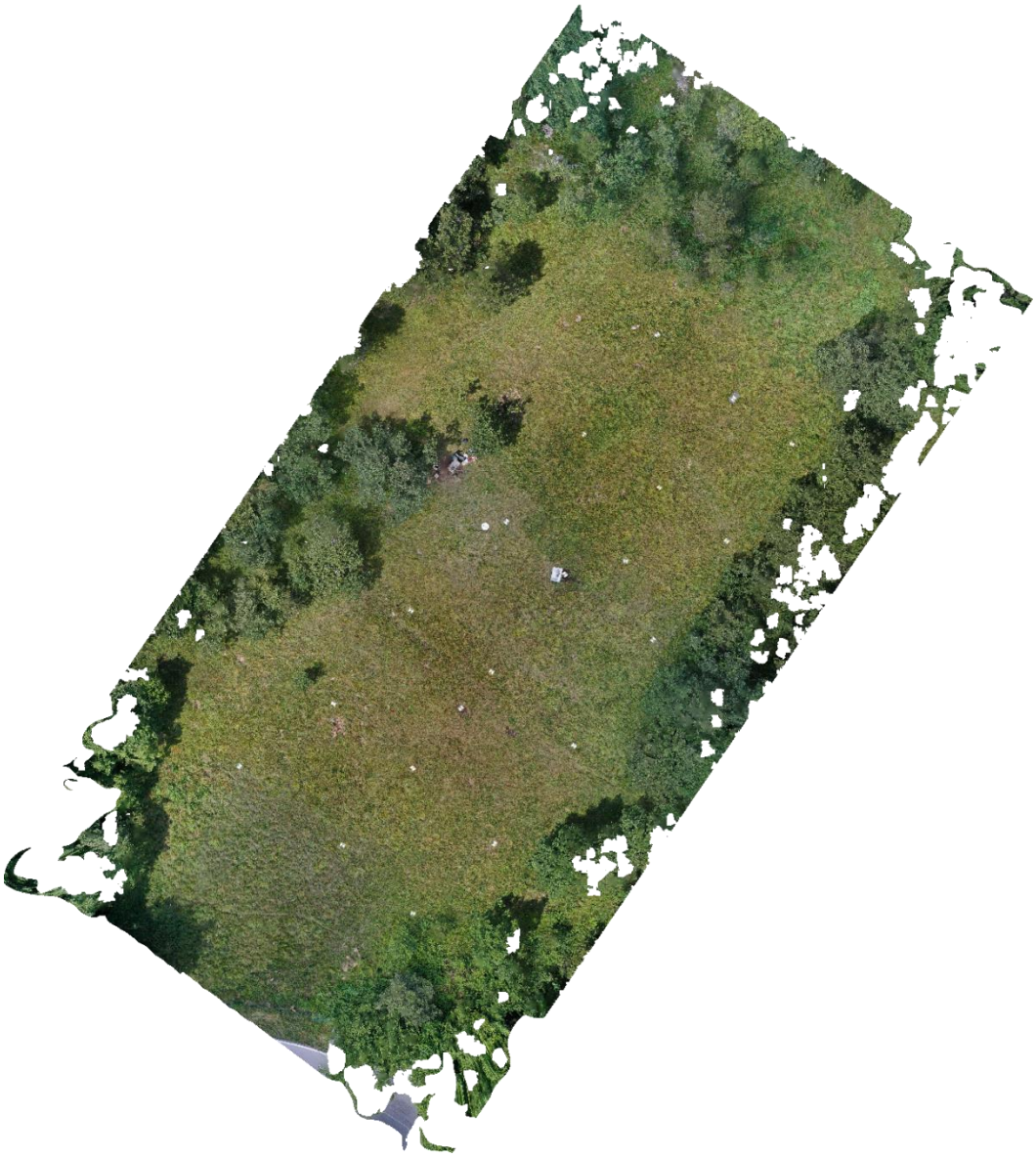

Figure 4-1: The overview of the Study Area

The average flying height was at 30 meters above ground with drone speed of 0.5 m/s. The flight of 10 strips resulted in an overlapping of 70% both across-track and along-track with total number of nadiral images being 87. All the obtained data was processed in Agisoft Metashape Pro (version 1.7.4.) with Local Reference System being chosen. The software performs camera self-calibration and obtained EO parameters by Aerial Triangulation technique.

Post-processing

Due to the fact that the aim of this project is to demonstrate accuracies of GCPs with different number and distribution, five configurations were proposed to be processed by U.Ph.O. tool and further compared with post-processing results from Agisoft Metashape software. Using the DSM of 5 meters, the tool was run. We acquire the first planning parameters by considering the associated restrictions on the planning and determining the strip direction:

- Flight altitude: 30 m.
- Scale frame 1: 3000
- GSD (m): 0.007 m.
- Ground projection W (m): 39.6
- Ground projection H (m): 26.4
- Distance of strip min. (m): 11.9
- Number of strips: 10
- Reel wheelbase (m): 10.821
- Base of intake (m): 7.92
- Maximum drone speed (0.1 m/sec): 39
- Strip length: 56.331

The results above are applied to all configuration, as well as the visibility map that is demonstrated in the Figure 4-2 showing the number of frames imaging each DSM pixel. From the figure it can be understood that the picture overlapping is up to 4 frames, yet having some area portions without any overlapping due to the fact that trees create significant obstacles. Since the resolution of the DSM is low (5 m.), these obstacles have then affected some GCPs to not have any value because they fall inside the same pixel as shadowed portions.

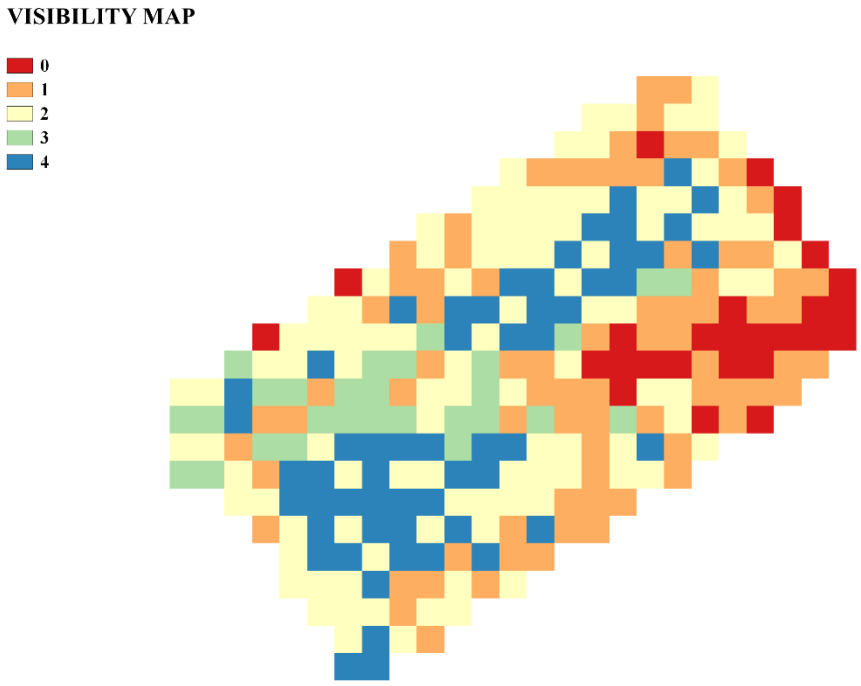

Figure 4-2: The visibility map

The following results demonstrate different outcomes of each configuration with different number of GCPs used.

Configuration 1

Figure 4-3: Configuration 1 - The distribution of GCPs

The first configuration involves 17 GCPs and 3 check points.
Eventually, the maps of predicted precisions are constructed using the methods described in Chapter 3 (The Unmanned Photogrammetric Office). The map constructed using the rigorous method is the most precise. Following figures demonstrate estimated precisions across the survey area.

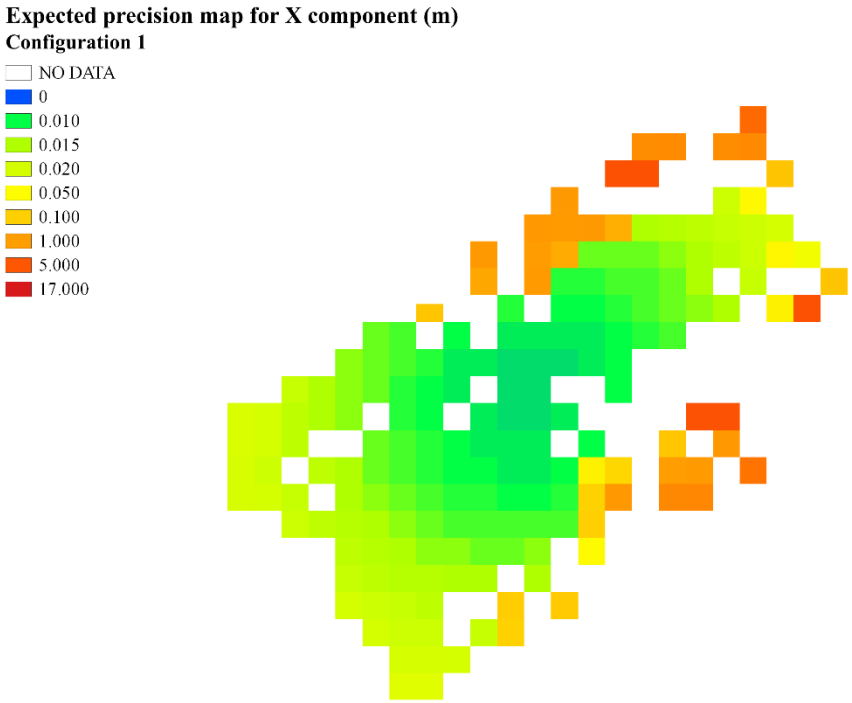

Figure 4-4: Configuration 1 - Map of expected precisions in X direction (in meters) obtained with rigorous method

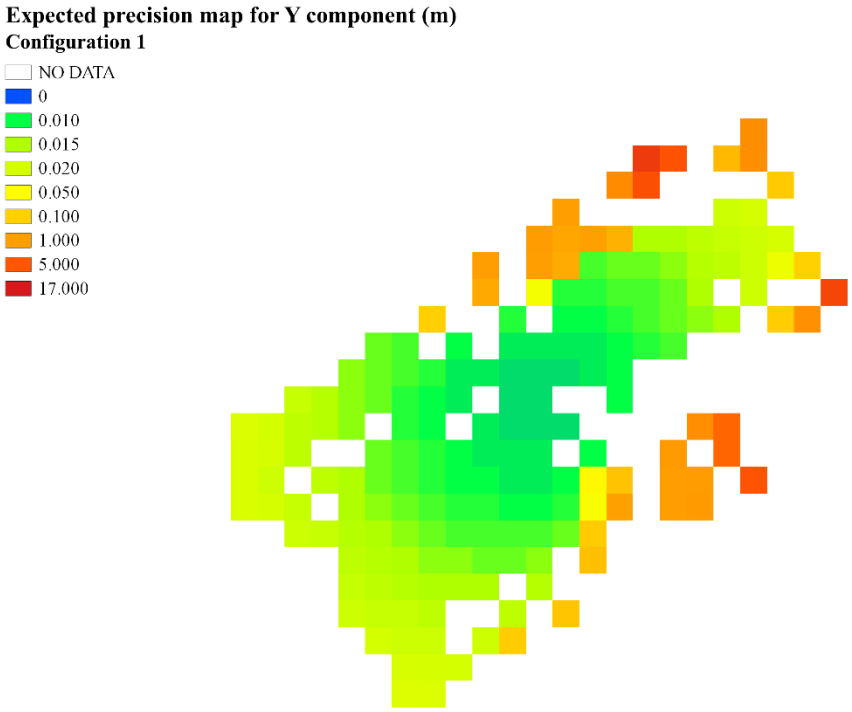

Figure 4-5: Configuration 1 - Map of expected precisions in Y direction (in meters) obtained with rigorous method

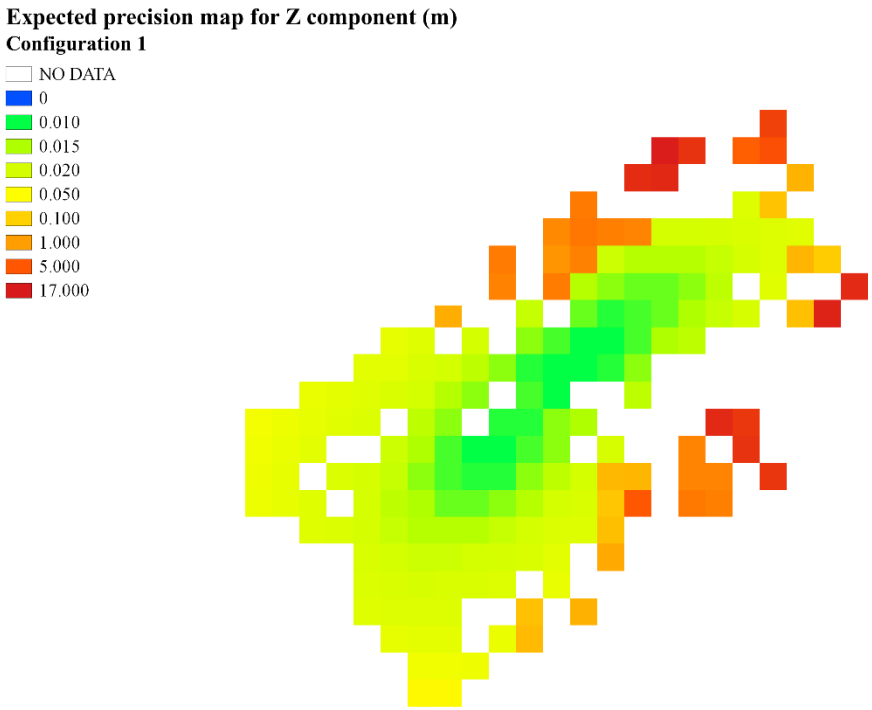

Figure 4-6: Configuration 1 - Map of expected precisions in Z direction (in meters) obtained with rigorous method

By analyzing Figures 4-4, 4-5, and 4-6, the following charts report the number of cells falling in each range of accuracy. It should be noted that class range is up to 3 mm, however, the values from 0.1 m are grouped in wider ranges.

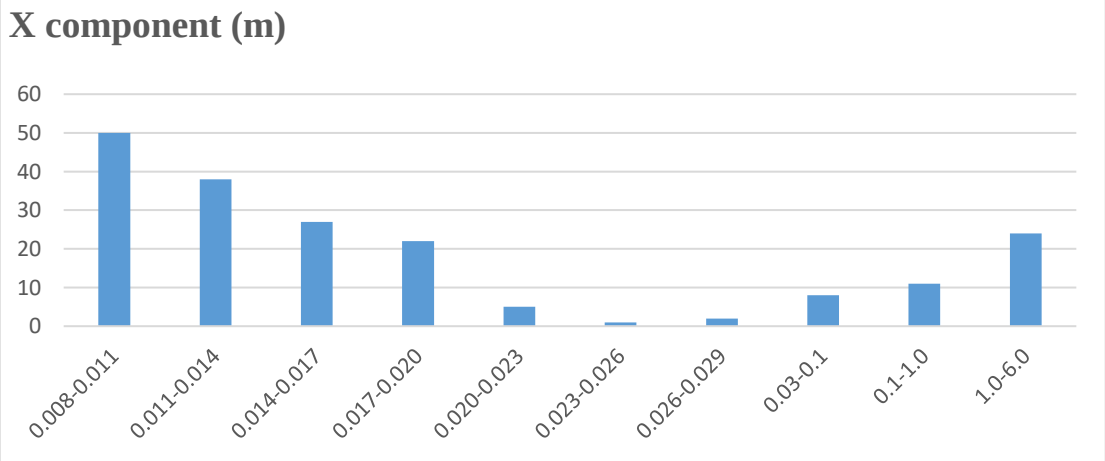

Chart 4-1: Configuration 1 - X component values grouped

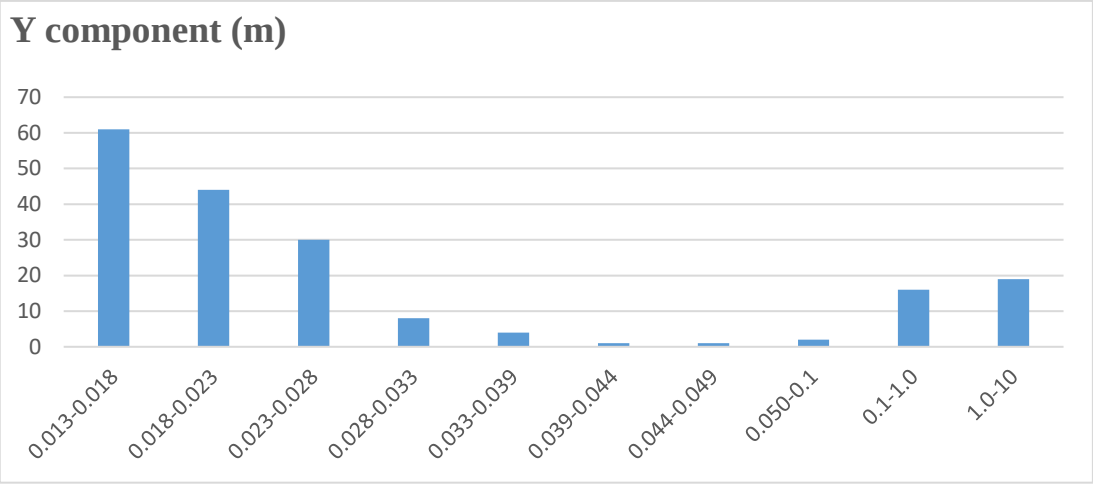

Chart 4-2: Configuration 1 - Y component values grouped

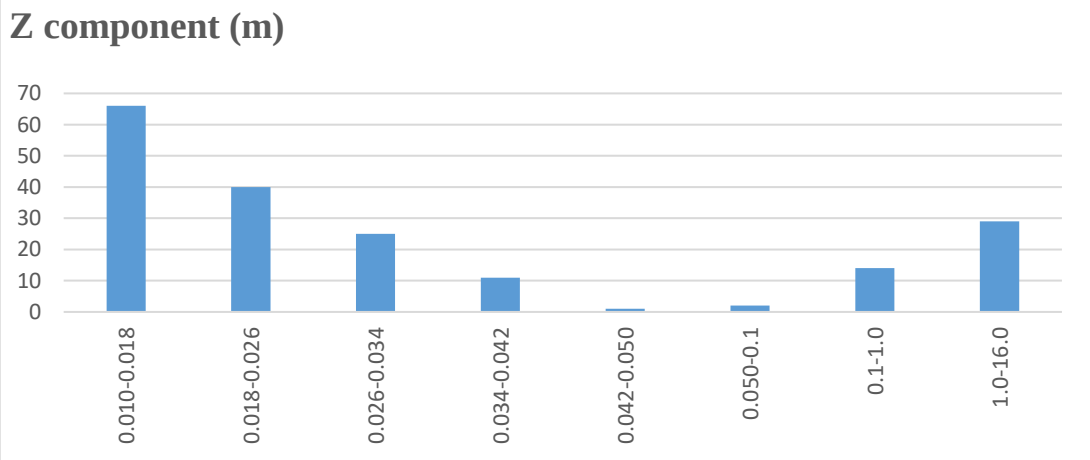

Chart 4-3: Configuration 1 - Z component values grouped

Moving from highest accuracies to lower ones the number of cells decreases. The first class range is the most dense with the highest number of cells in it, while values higher than 1 m should be considered as outliers.
The following table shows estimated precision per each marker distributed across the survey area.

Marker	GCP/CP	X error (mm)	Y error (mm)	Z error (mm)
1	1	14	14	18
2	1	13	13	14
3	1	13	13	16
4	1	11	11	14
5	0	11	11	12
6	1	NaN	NaN	NaN
7	1	NaN	NaN	NaN
8	0	8	8	10

Marker	GCP/CP	X error (mm)	Y error (mm)	Z error (mm)
9	1	NaN	NaN	NaN
10	1	9	9	14
11	1	8	8	11
12	1	NaN	NaN	NaN
13	1	10	10	16
14	0	10	10	10
15	1	10	10	14
16	1	13	13	19
17	1	12	12	13
18	1	14	14	20
19	1	8	8	11
20	1	9	09	10
Total GCPs error		11	11	15
Total CP error		10	10	11

Table 4-1: Configuration 1 - Estimated precision of each marker

In the table above, the values of 1 and 0 in the second column are related to the GCPs and Check Points, respectively.
Following the results estimated by U.Ph.O., it can be observed that average GCP accuracy along X-axis, Y-axis, and Z-axis are 11 mm, 11mm, and 15 mm respectively, while Check Points have errors of 10 mm, 10 mm, and 11 mm along X,Y, and Z axis respectively.
Having obtained estimated precisions and deciding that the results are adequate to run the survey, the post-processing part was carried out in Agisoft Metashape Pro.
Alignment parameters in the software were set to high accuracy, resulting in a point cloud of 814908 points that took around 20 minutes to give accuracy values. After using camera optimization tool, the Dense Cloud, Mesh, Texture, DSM, and Orthophoto were generated and were chosen to be at high quality for every configuration.
Following table shows results obtained by Agisoft Metashape Pro, where the signed values are coherent with direction of positive axis.

Marker	GCP/CP	X (m)	Y (m)	Z (m)	X error (mm)	Y error (mm)	Z error (mm)
7	1	400097.348	4000110.152	300.66	-8	-2	-7
6	1	400105.482	4000119.341	300.713	-5	-1	5
8	0	400103.481	4000104.604	300.052	2	-1	-21
5	0	400113.389	4000113.746	300.371	-2	-12	-21
20	1	400109.837	4000105.982	300.125	16	1	-4
4	1	400120.517	4000108.118	299.953	7	-6	-10

Marker	GCP/CP	X (m)	Y (m)	Z (m)	X error (mm)	Y error (mm)	Z error (mm)
9	1	400112.762	4000097.709	299.691	8	-7	1
1	1	400113.237	4000129.847	300.947	-16	-8	-3
2	1	400121.206	4000123.12	300.353	-4	-3	-20
3	1	400127.429	4000118.316	300.12	-6	-9	23
12	1	400087.261	4000100.751	300.545	2	6	10
11	1	400095.744	4000094.343	300.062	-6	1	-1
10	1	400104.407	4000086.538	299.49	9	3	35
19	1	400092.527	4000090.5	299.769	4	4	-10
13	1	400079.105	4000090.941	300.528	-10	14	-1
18	1	400069.25	4000084.353	300.937	-31	13	13
14	0	400087.457	4000084.163	299.891	2	7	-15
17	1	400080.054	4000076.054	299.792	0	2	-1
15	1	400096.036	4000076.199	299.423	24	-1	-21
16	1	400087.465	4000068.902	299.417	17	-6	-7
Total GCP error					13	7	14
Total CP error					2	8	20

Table 4-2: Configuration 1 - Empirical precision of each marker

Configuration 2

Figure 4-7: Configuration 2 – The distribution of GCPs

The second configuration involves 14 GCPs and 6 check points. Here, the GCPs are placed along the borders of the survey area, while check points are chosen to be those markers that are in the center.

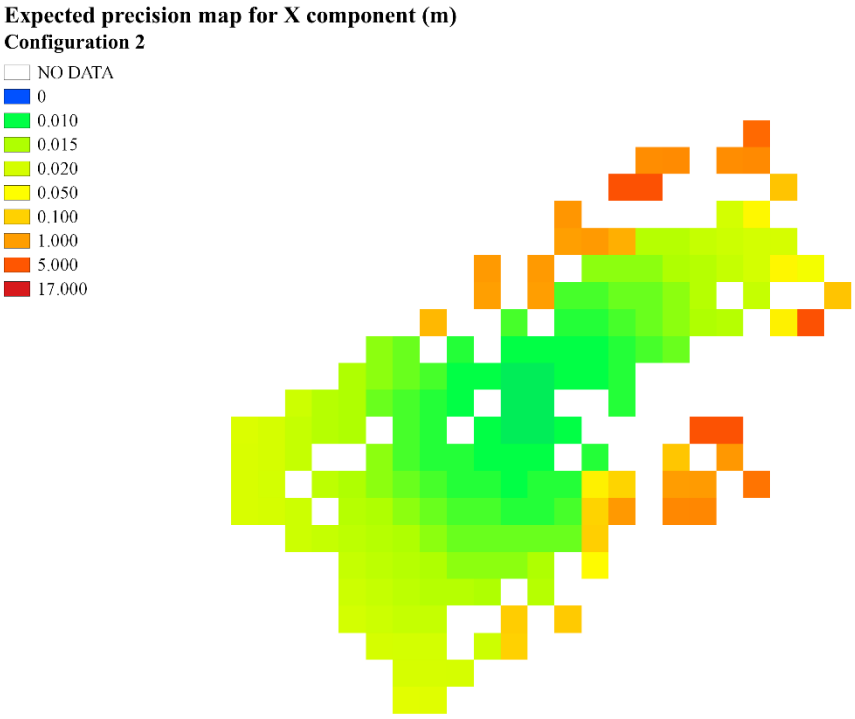

Figure 4-8: Configuration 2 - Map of expected precisions in X direction (in meters) obtained with rigorous method

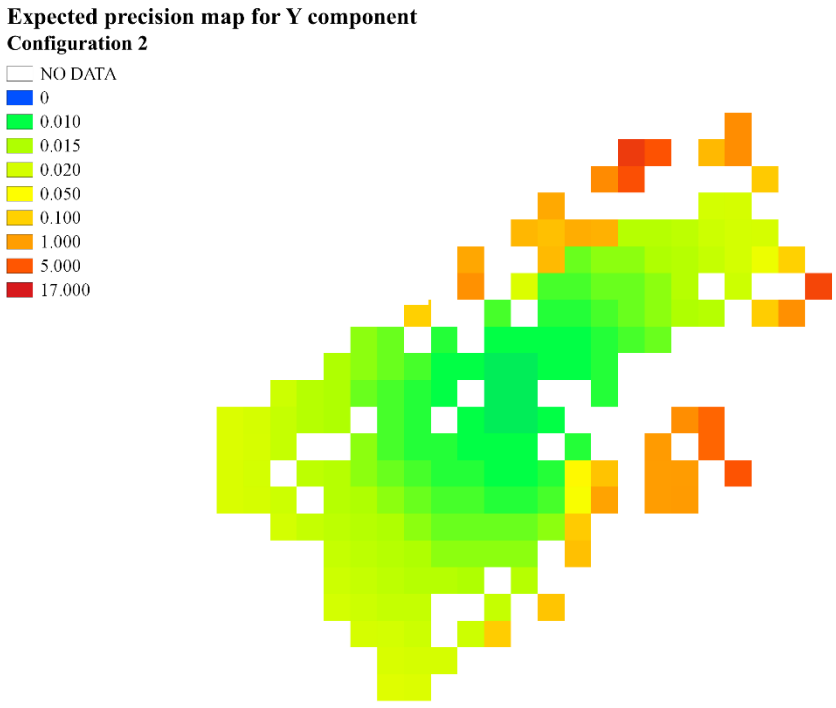

Figure 4-9: Configuration 2 - Map of expected precisions in Y direction (in meters) obtained with rigorous method

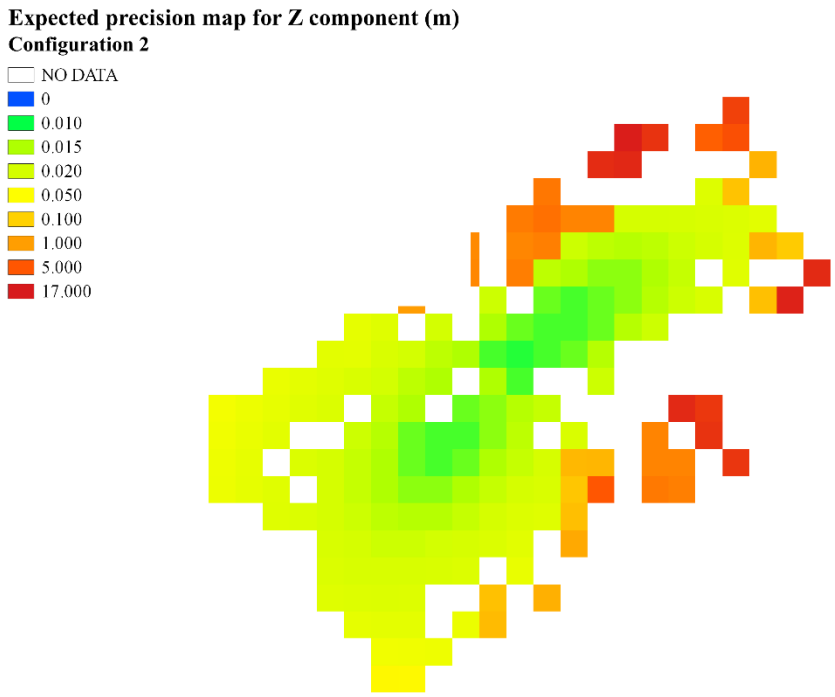

Figure 4-10: Configuration 2 - Map of expected precisions in Z direction (in meters) obtained with rigorous method

By analyzing Figures 4-8, 4-9, and 4-10, the following charts report the number of cells falling in each range of accuracy. It should be noted that class range is up to 3 mm, however, the values from 0.1 m are grouped in wider ranges.

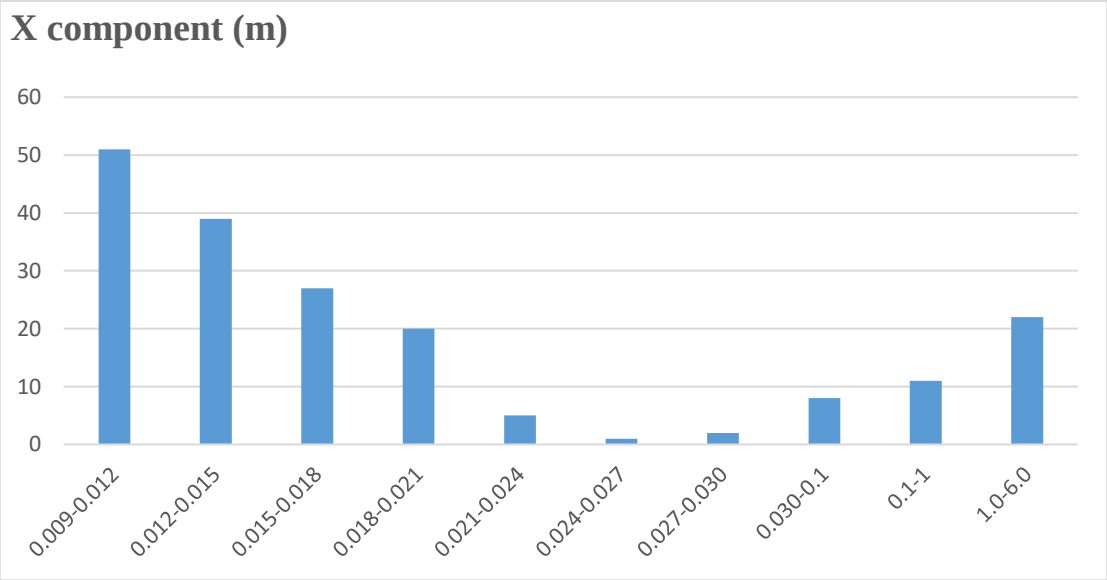

Chart 4-4: Configuration 2 - X component values grouped

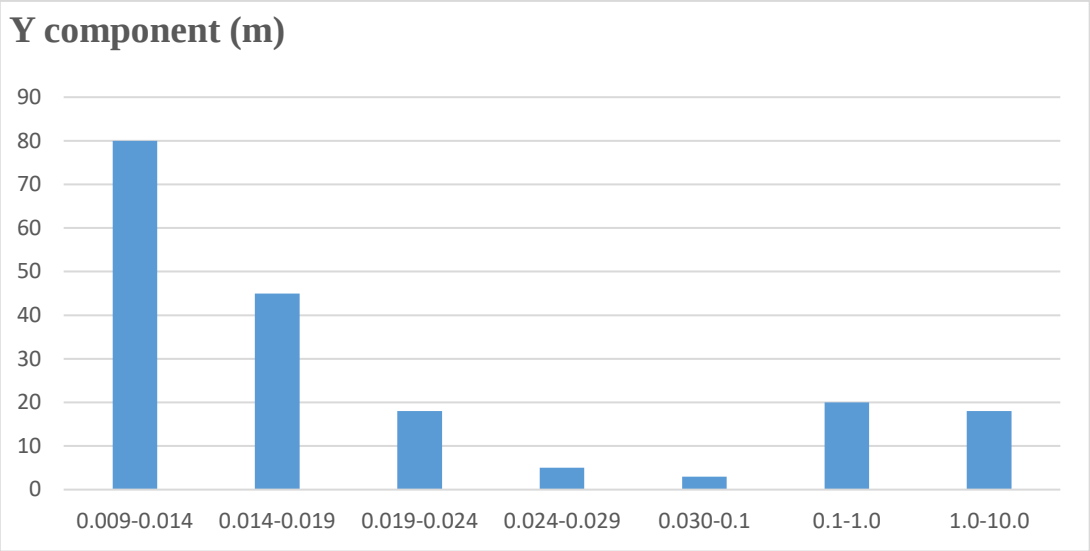

Chart 4-5: Configuration 2 - Y component values grouped

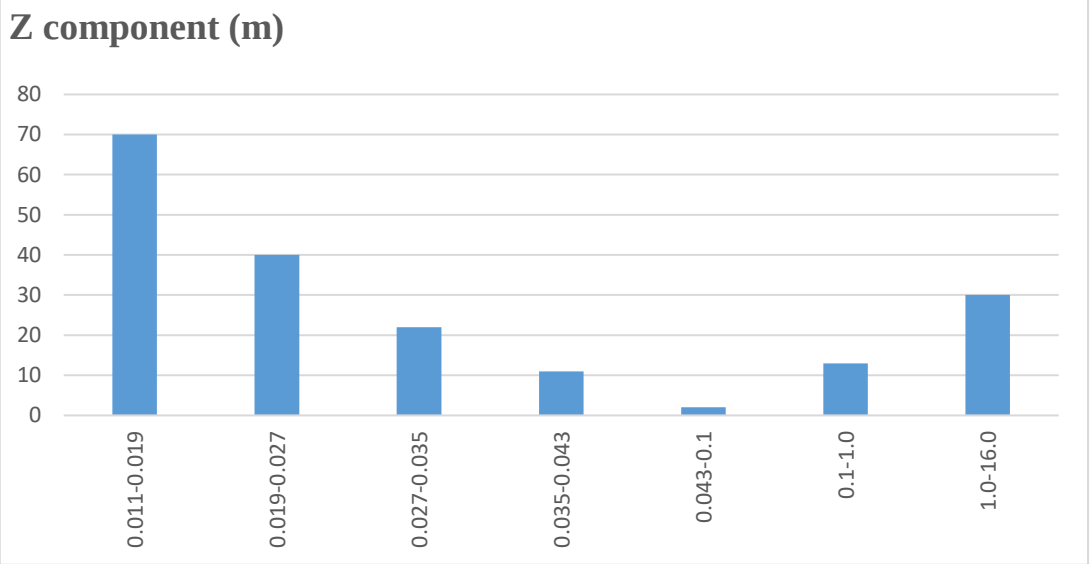

Chart 4-6: Configuration 2 - Z component values grouped

Moving from highest accuracies to lower ones the number of cells decreases. The first class range is the most dense with the highest number of cells in it. Values higher than 1 m should be considered as outliers.

The following table shows estimated precision per each marker distributed across the survey area.

Marker	GCP/CP	X (mm)	Y (mm)	Z (mm)
1	1	15	15	19
2	1	14	14	15
3	1	14	14	16
4	1	12	12	15
5	0	12	12	13
6	1	NaN	NaN	NaN
7	1	NaN	NaN	NaN
8	0	10	10	12
9	1	NaN	NaN	NaN
10	1	10	10	15
11	0	0.009	9	14
12	1	NaN	NaN	NaN
13	1	11	11	18
14	0	11	11	12
15	1	11	11	15
16	1	14	14	19
17	1	13	13	14
18	1	14	14	20
19	0	9	9	14
20	0	10	10	12
Total GCPs error		13	13	17
Total CP error		10	10	13

Table 4-3: Configuration 2 - Estimated precision of each marker

In the table above, the values of 1 and 0 in the second column are related to the GCPs and Check Points, respectively.
Following the results estimated by U.Ph.O., it can be observed that average accuracy along X-axis, Y-axis, and Z-axis are 13 mm, 13 mm, and 17 mm respectively, while Check Points have errors of 10 mm, 10 mm, and 13 mm along X,Y, and Z axis respectively.
Following table shows simulation results obtained by Agisoft Metashape Pro, where the signed values are coherent with direction of positive axis.

Marker	GCP/CP	X (m)	Y (m)	Z (m)	X error (mm)	Y error (mm)	Z error (mm)
7	1	400097.3	4000110	300.66	-7	-2	-10
6	1	400105.5	4000119	300.713	-4	-1	3
8	0	400103.5	4000105	300.052	3	0	-26
5	0	400113.4	4000114	300.371	-1	-11	-24
20	0	400109.8	4000106	300.125	18	1	-9
4	1	400120.5	4000108	299.953	8	-6	-11
9	1	400112.8	4000098	299.691	9	-6	-2

Marker	GCP/CP	X (m)	Y (m)	Z (m)	X error (mm)	Y error (mm)	Z error (mm)
1	1	400113.2	4000130	300.947	-15	-7	-1
2	1	400121.2	4000123	300.353	-2	-3	-19
3	1	400127.4	4000118	300.12	-5	-9	24
12	1	400087.3	4000101	300.545	3	7	7
11	0	400095.7	4000094	300.062	-5	1	-6
10	1	400104.4	4000087	299.49	10	3	32
19	0	400092.5	4000091	299.769	5	4	-15
13	1	400079.1	4000091	300.528	-10	14	-3
18	1	400069.3	4000084	300.937	-31	14	14
14	0	400087.5	4000084	299.891	3	7	-18
17	1	400080.1	4000076	299.792	1	3	-2
15	1	400096	4000076	299.423	25	-1	-23
16	1	400087.5	4000069	299.417	17	-7	-7
Total GCP error					13	7	15
Total CP error					8	6	18

Table 4-4: Configuration 2 - Empirical precision of each marker

Configuration 3

Figure 4-11: Configuration 3 – The distribution of GCPs

The third configuration involves 6 GCPs and 14 check points. Here, the GCPs are arranged along a straight line, while check points are chosen to be those markers along the borders. This configuration is wrong in photogrammetric point of view, but it was analyzed in order to study the behaviour of accuracy also in this case.

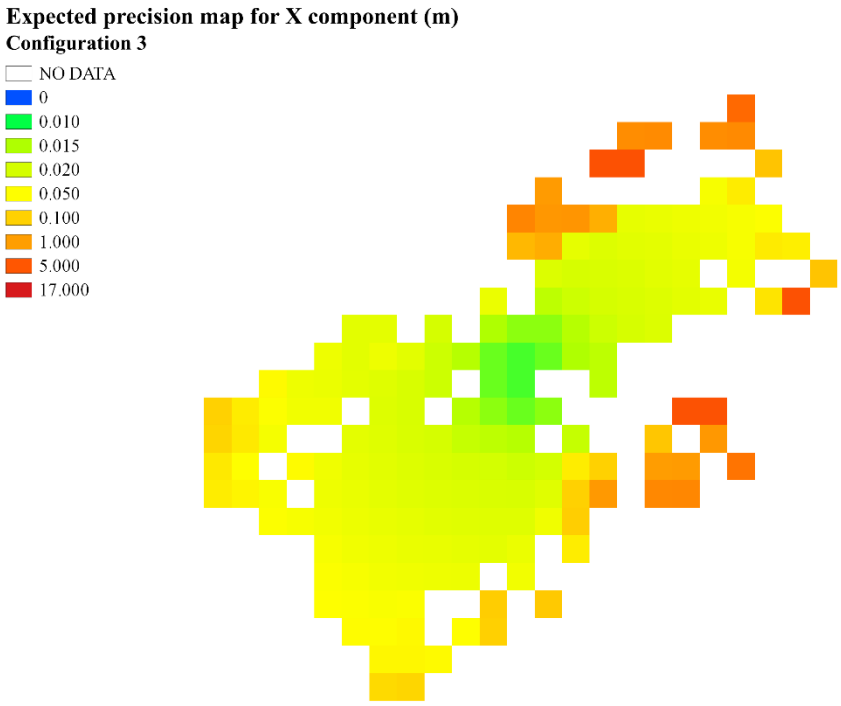

Figure 4-12: Configuration 3 - Map of expected precisions in X direction (in meters) obtained with rigorous method

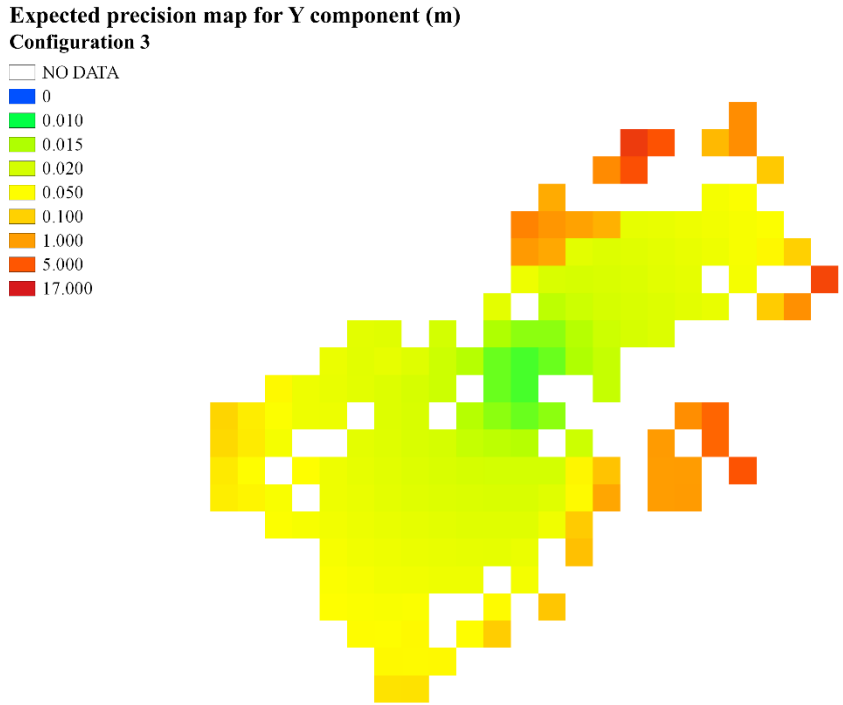

Figure 4-13: Configuration 3 - Map of expected precisions in Y direction (in meters) obtained with rigorous method

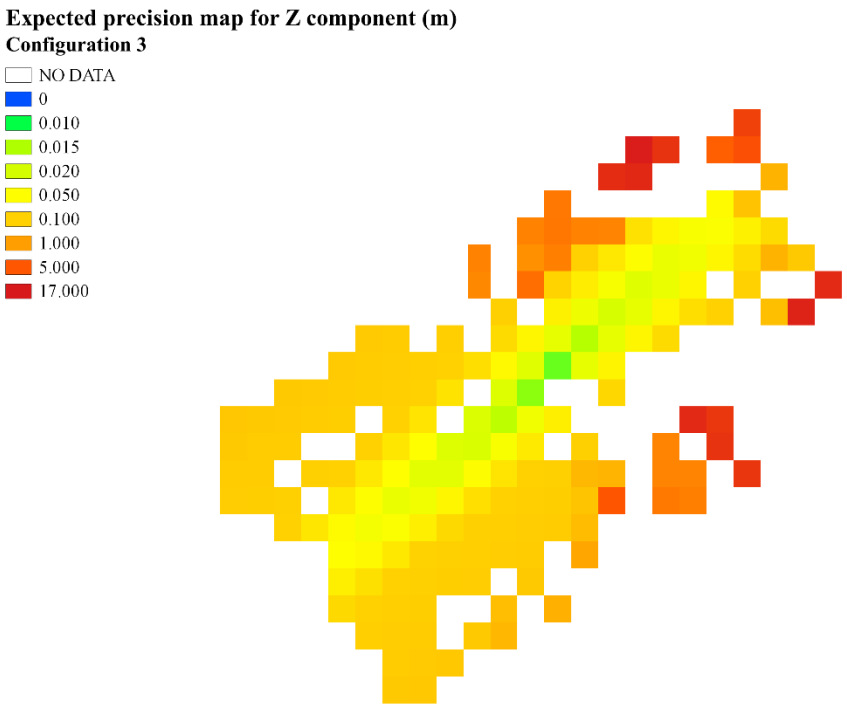

Figure 4-14: Configuration 3 - Map of expected precisions in Z direction (in meters) obtained with rigorous method

By analyzing Figures 4-12, 4-13, and 4-14, the following charts report the number of cells falling in each range of accuracy. It should be noted that class range is up to 3 mm, however, the values from 0.1 m are grouped in wider ranges.

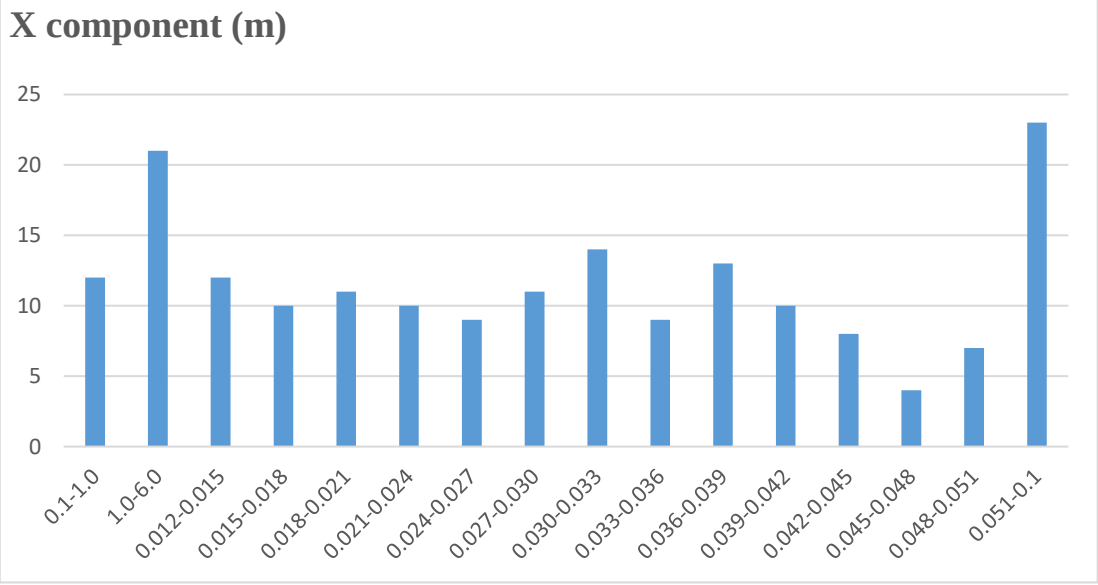

Chart 4-7: Configuration 3 - X component values grouped

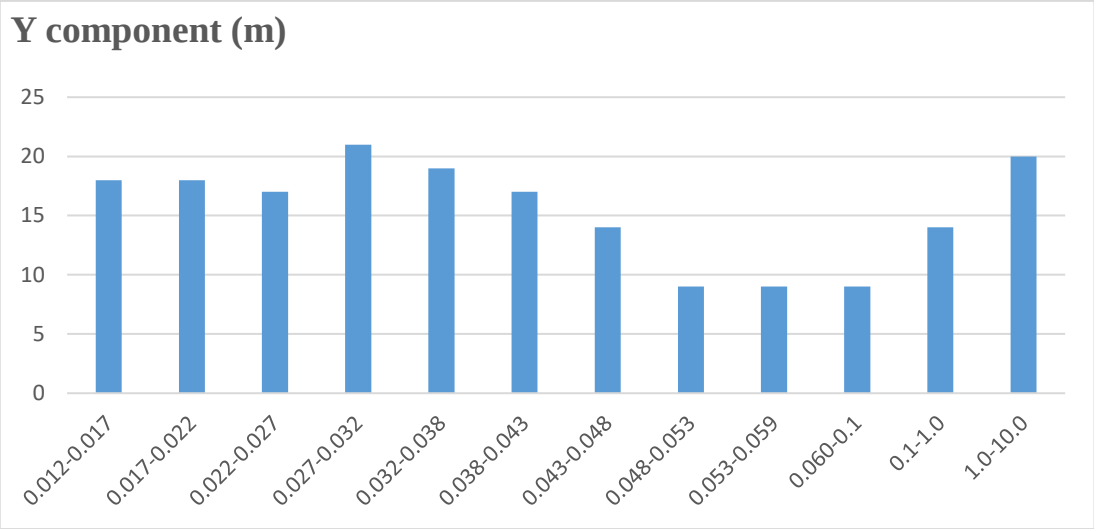

Chart 4-8: Configuration 3 - Y component values grouped

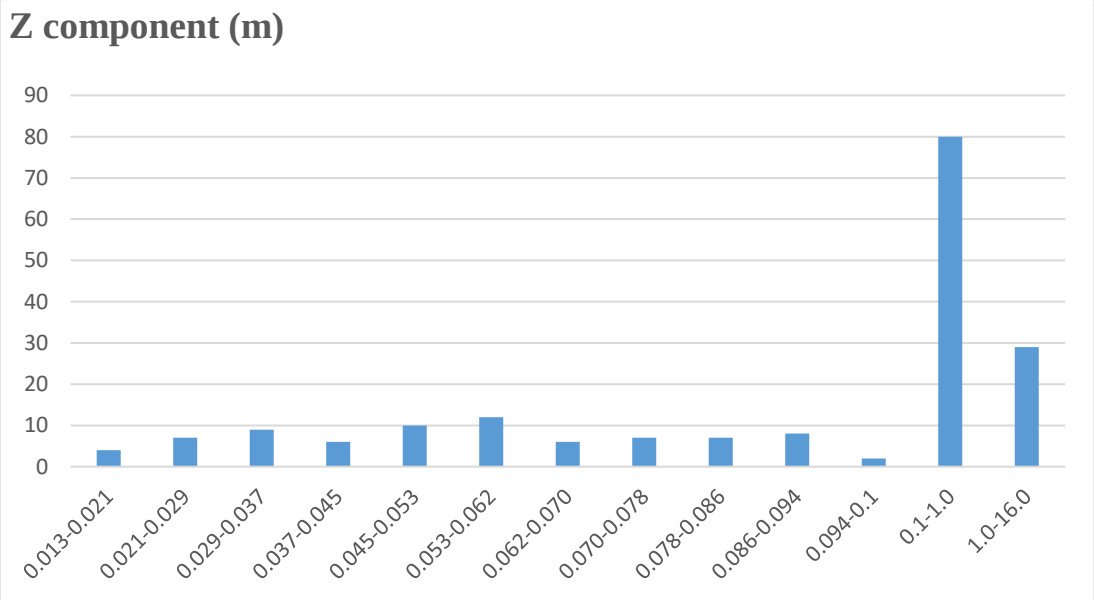

Chart 4-9: Configuration 3 - Z component values grouped

Unlike the first two configurations, planimetric accuracies remain at the same level starting to lose the number of cells reaching the values of 0.1 m. The altimetric accuracy shows very low results in general with class range between 0.1 m and 1 m being the most dense group. Values higher than 1 m should be considered as outliers. The following table shows estimated precision per each marker distributed across the survey area.

Marker	GCP/CP	X (mm)	Y (mm)	Z (mm)
1	0	31	31	87
2	0	30	30	36
3	0	30	29	52
4	0	22	22	70
5	1	21	21	22
6	0	NaN	NaN	NaN
7	0	NaN	NaN	NaN
8	1	13	13	13
9	0	NaN	NaN	NaN
10	0	16	16	86
11	1	14	14	17
12	0	NaN	NaN	NaN
13	0	24	24	112
14	1	21	21	26
15	0	23	23	80
16	0	32	32	106
17	0	29	29	40
18	0	35	35	125
19	1	14	14	17
20	1	16	16	16
Total GCPs error		17	16	19
Total CP error		27	27	80

Table 4-5: Configuration 3 - Estimated precision of each marker

In the table above, the values of 1 and 0 in the second column are related to the GCPs and Check Points, respectively.
Following the results estimated by U.Ph.O., it can be observed that average accuracy along X-axis, Y-axis, and Z-axis are 17 mm, 16 mm, and 19 mm respectively, while Check Points have errors of 27 mm, 27 mm, and 80 mm along X,Y, and Z axis respectively.
Following table shows simulation results obtained by Agisoft Metashape Pro, where the signed values are coherent with direction of positive axis.

Marker	GCP/CP	X (m)	Y (m)	Z (m)	X error (mm)	Y error (mm)	Z error (mm)
7	0	400097.3	4000110	300.66	-12	-3	50
6	0	400105.5	4000119	300.713	-11	1	73
8	1	400103.5	4000105	300.052	-2	2	-4
5	1	400113.4	4000114	300.371	-7	-6	2
20	1	400109.8	4000106	300.125	13	5	-1

Marker	GCP/CP	X (m)	Y (m)	Z (m)	X error (mm)	Y error (mm)	Z error (mm)
4	0	400120.5	4000108	299.953	5	2	-28
9	0	400112.8	4000098	299.691	7	-2	-31
1	0	400113.2	4000130	300.947	-25	-4	92
2	0	400121.2	4000123	300.353	-11	5	23
3	0	400127.4	4000118	300.12	-13	2	43
12	0	400087.3	4000101	300.545	-1	2	75
11	1	400095.7	4000094	300.062	-7	-1	8
10	0	400104.4	4000087	299.49	9	4	3
19	1	400092.5	4000091	299.769	2	1	-1
13	0	400079.1	4000091	300.528	-13	5	67
18	0	400069.3	4000084	300.937	-33	-1	119
14	1	400087.5	4000084	299.891	1	0	-2
17	0	400080.1	4000076	299.792	-1	-10	25
15	0	400096	4000076	299.423	29	-7	-67
16	0	400087.5	4000069	299.417	20	-20	-31
Total GCP error					7	3	4
Total CP error					17	7	60

Table 4-6: Configuration 3- Empirical precision of each marker

Configuration 4

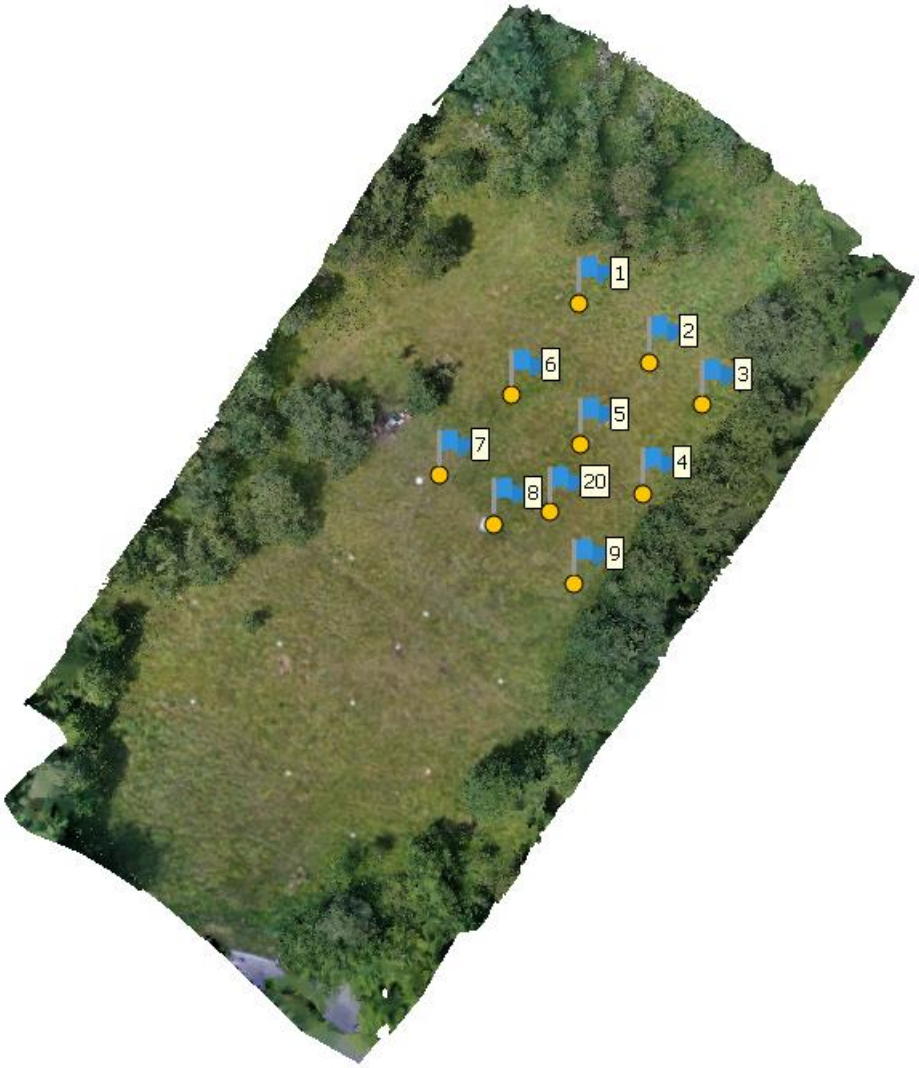

Figure 4-15: Configuration 4 – The distribution of GCPs

The fourth configuration involves 10 GCPs and 10 check points. Here, the GCPs are located in the first half of the survey area, while check points are on the other half.

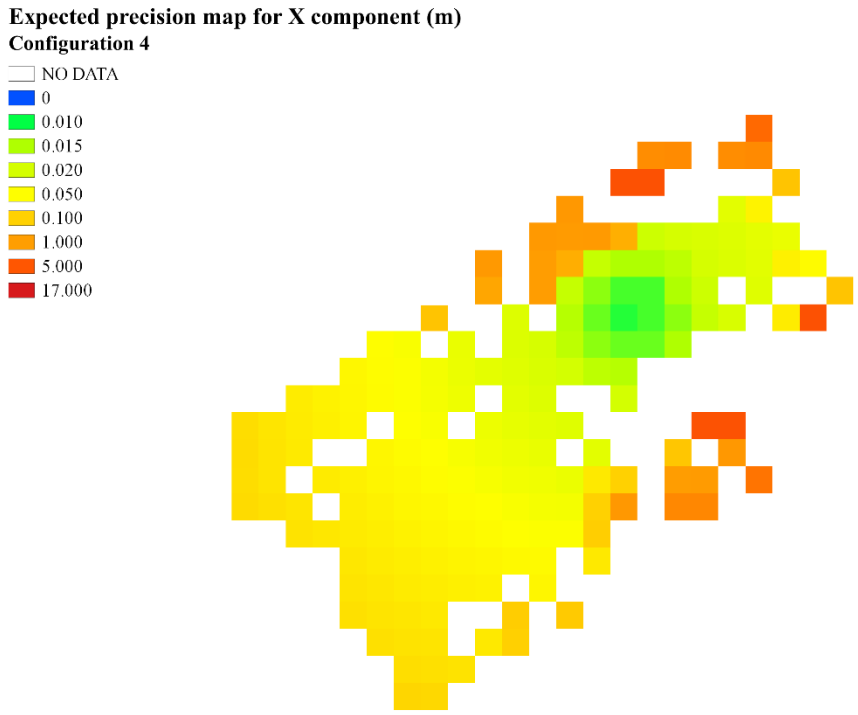

Figure 4-16: Configuration 4 - Map of expected precisions in X direction (in meters) obtained with rigorous method

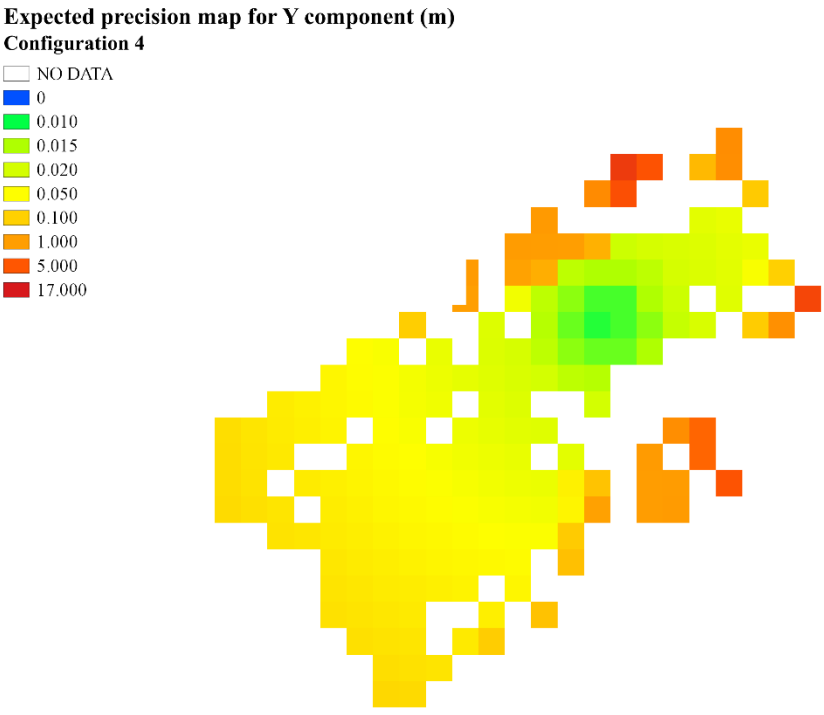

Figure 4-17: Configuration 4 - Map of expected precisions in Y direction (in meters) obtained with rigorous method

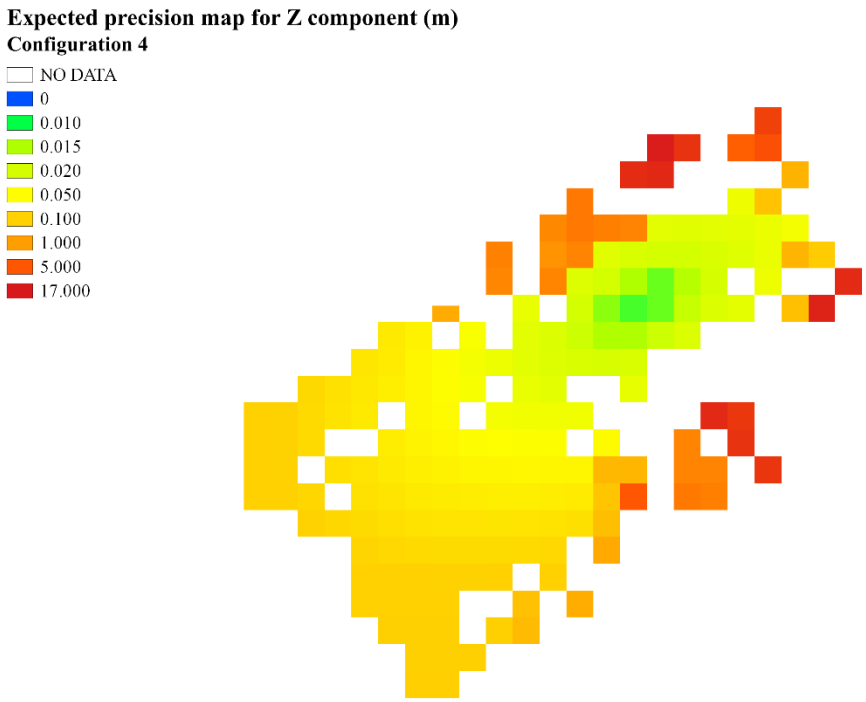

Figure 4-18: Configuration 4 - Map of expected precisions in Z direction (in meters) obtained with rigorous method

By analyzing Figures 4-16, 4-17, and 4-18, the following charts report the number of cells falling in each range of accuracy. It should be noted that class range is up to 3 mm, however, the values from 0.1 m are grouped in wider ranges.

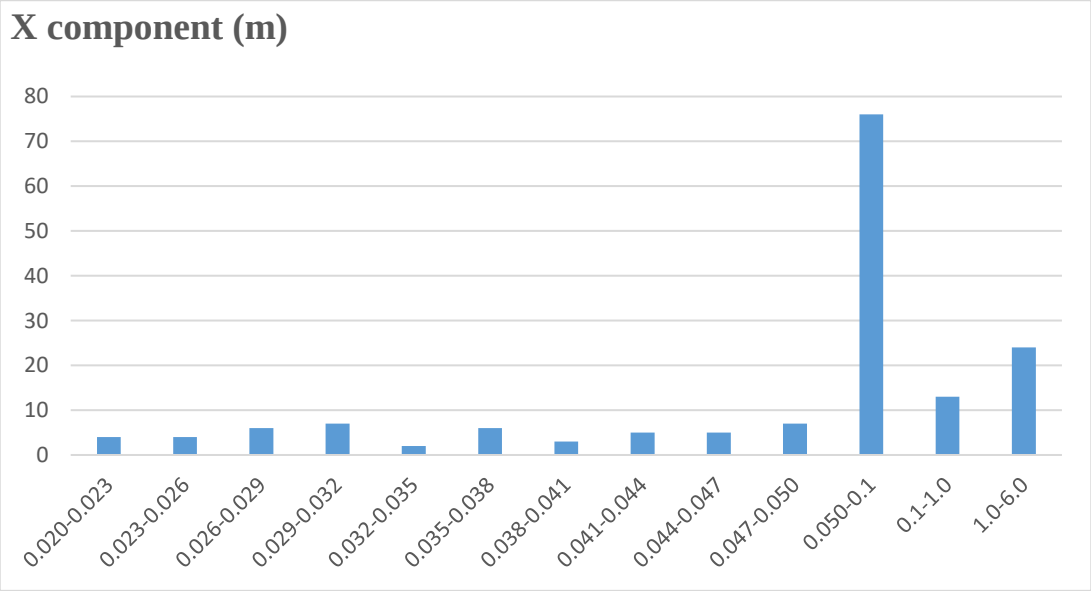

Chart 4-10: Configuration 4 - X component values grouped

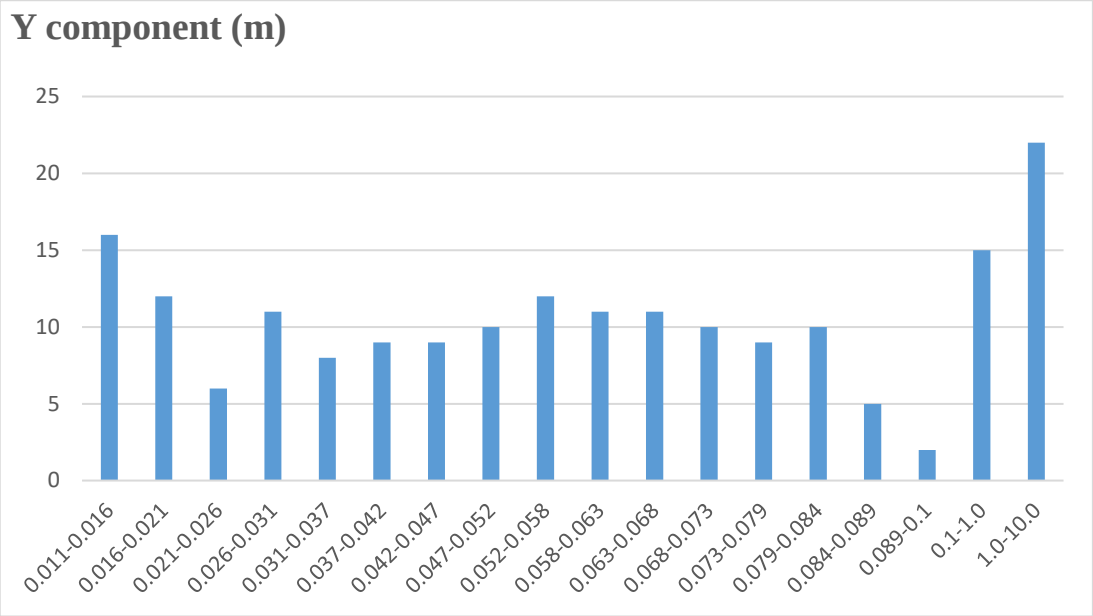

Chart 4-11: Configuration 4 - Y component values grouped

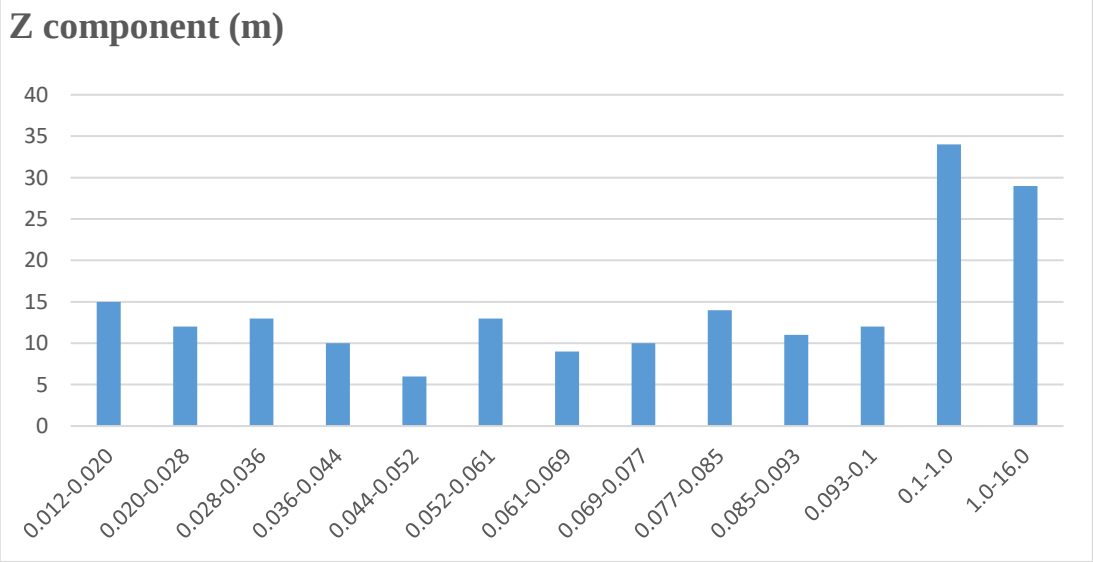

Chart 4-12: Configuration 4 - Z component values grouped

Both planimetric and altimetric accuracies of this configuration remain at almost the same level until reaching 0.1 m. Except for the case of X component, where a majority of cells are concentrated in the range between 0.05 m and 0.1 m. Values higher than 1 m should be considered as outliers.

The following table shows estimated precision per each marker distributed across the survey area.

Marker	GCP/CP	X (mm)	Y (mm)	Z (mm)
1	1	18	18	25
2	1	15	15	16
3	1	15	15	20
4	1	14	14	20
5	1	11	11	12
6	1	NaN	NaN	NaN
7	1	NaN	NaN	NaN
8	1	20	20	23
9	1	NaN	NaN	NaN
10	0	32	33	38
11	0	34	34	41
12	0	NaN	NaN	NaN
13	0	47	46	68
14	0	45	45	53
15	0	47	47	54
16	0	59	59	69
17	0	57	56	71
18	0	62	61	89
19	0	34	34	41
20	1	14	14	15
Total GCPs error		15	15	19
Total CP error		46	46	58

Table 4-7: Configuration 4 - Estimated precision of each marker

In the table above, the values of 1 and 0 in the second column are related to the GCPs and Check Points, respectively.
Following the results estimated by U.Ph.O., it can be observed that average GCP accuracy along X-axis, Y-axis, and Z-axis are 15 mm., 15 mm., and 19 mm. respectively, while Check Points have errors of 46 mm, 46 mm, and 58 mm along X,Y, and Z axis respectively.
Following table shows simulation results obtained by Agisoft Metashape Pro, where the signed values are coherent with direction of positive axis.

Marker	GCP/CP	X (m)	Y (m)	Z (m)	X error (mm)	Y error (mm)	Z error (mm)
7	1	400097.3	4000110	300.66	-10	6	-5
6	1	400105.5	4000119	300.713	-3	6	23
8	1	400103.5	4000105	300.052	1	6	-10
5	1	400113.4	4000114	300.371	-1	-7	3
20	1	400109.8	4000106	300.125	15	6	11

Marker	GCP/CP	X (m)	Y (m)	Z (m)	X error (mm)	Y error (mm)	Z error (mm)
4	1	400120.5	4000108	299.953	6	-4	-4
9	1	400112.8	4000098	299.691	5	-1	-5
1	1	400113.2	4000130	300.947	-10	-1	-9
2	1	400121.2	4000123	300.353	1	-1	-17
3	1	400127.4	4000118	300.12	-4	-9	13
12	0	400087.3	4000101	300.545	-4	17	-52
11	0	400095.7	4000094	300.062	-10	10	-52
10	0	400104.4	4000087	299.49	3	13	-31
19	0	400092.5	4000091	299.769	0	15	-95
13	0	400079.1	4000091	300.528	-21	25	-170
18	0	400069.3	4000084	300.937	-51	24	-289
14	0	400087.5	4000084	299.891	-5	18	-173
17	0	400080.1	4000076	299.792	-9	16	-280
15	0	400096	4000076	299.423	20	12	-216
16	0	400087.5	4000069	299.417	10	7	-319
Total GCP error					7	5	12
Total CP error					20	17	196

Table 4-8: Configuration 4 - Empirical precision of each marker

Configuration 5

Figure 4-19: Configuration 5 – The distribution of GCPs

The fifth configuration involves 5 GCPs and 15 check points. Here, five GCPs were chosen, four of them being located from four edges, while the fifth one was located in the center of the survey area.

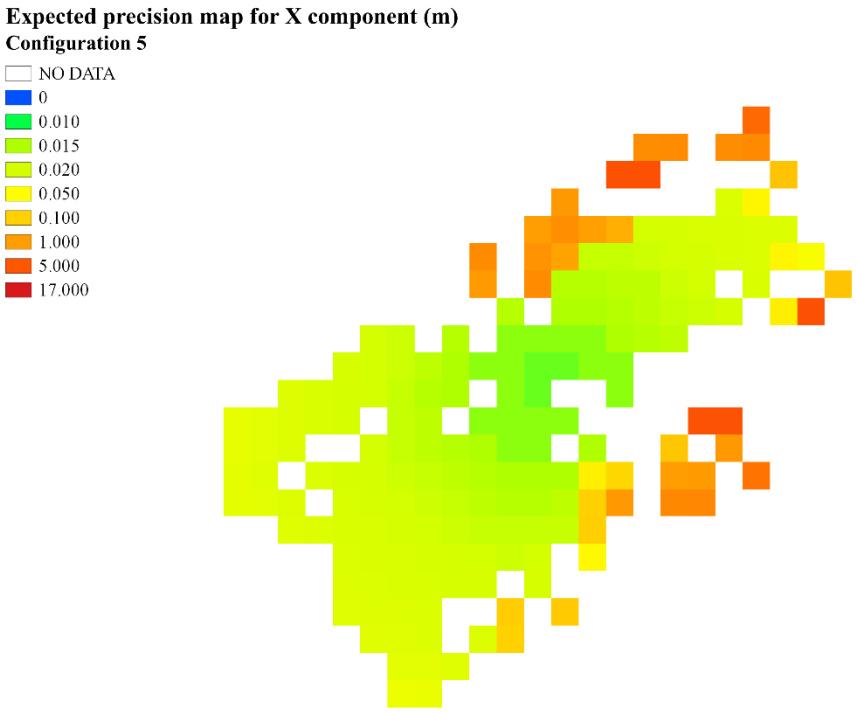

Figure 4-20: Configuration 5 - Map of expected precisions in X direction (in meters) obtained with rigorous method

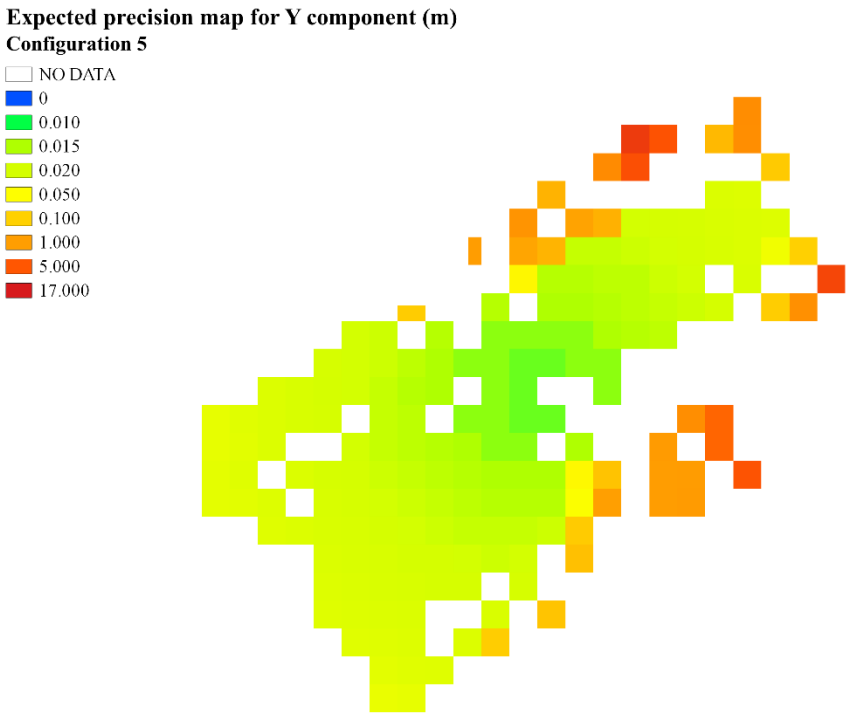

Figure 4-21: Configuration 5 - Map of expected precisions in Y direction (in meters) obtained with rigorous method

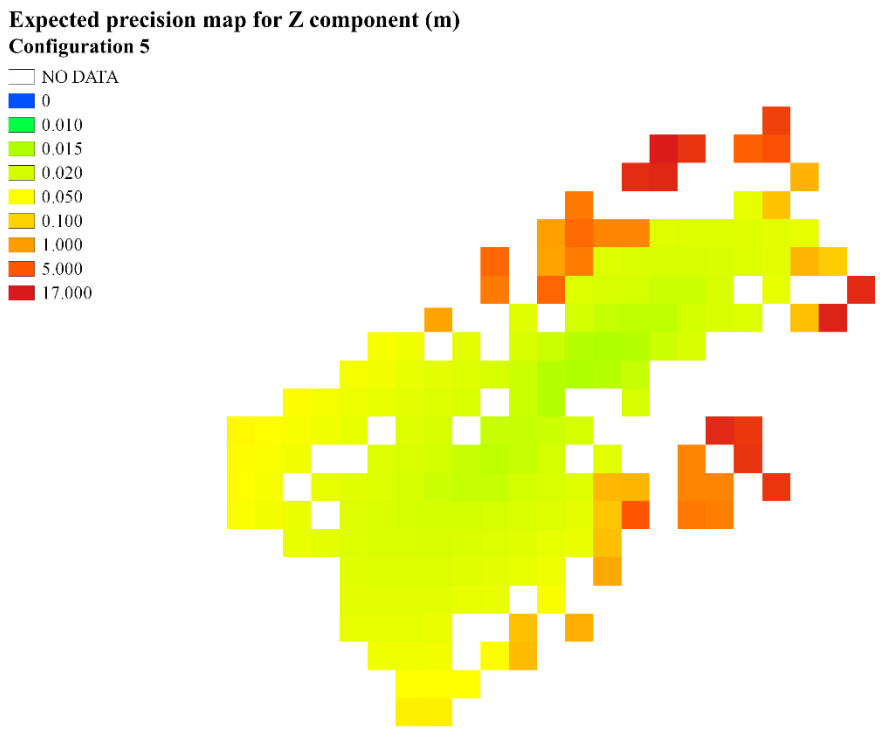

Figure 4-22: Configuration 5 - Map of expected precisions in Z direction (in meters) obtained with rigorous method

By analyzing Figures 4-20, 4-21, and 4-22, the following charts report the number of cells falling in each range of accuracy. It should be noted that class range is up to 3 mm, however, the values from 0.1 m are grouped in wider ranges.

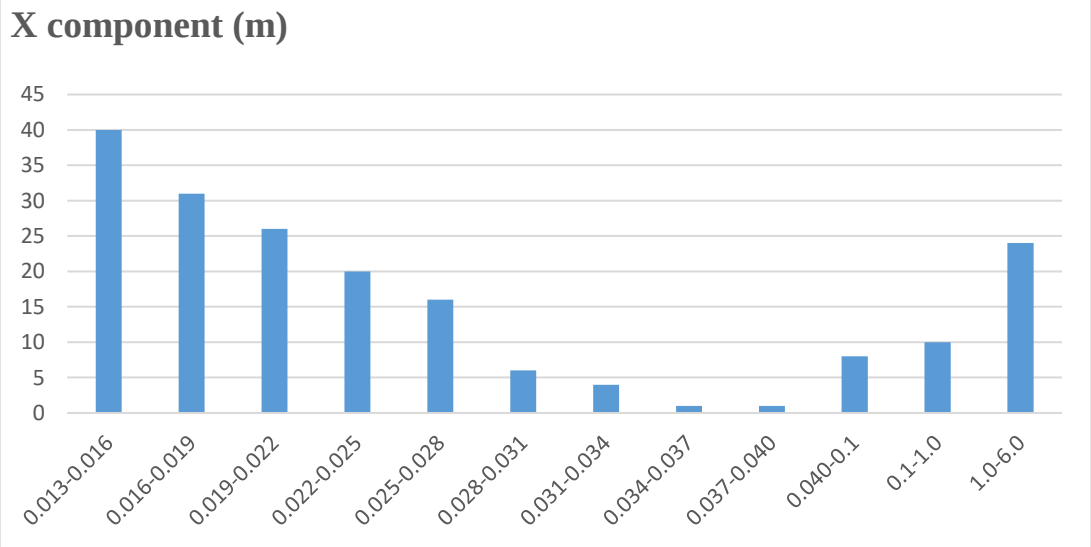

Chart 4-13: Configuration 5 - X component values grouped

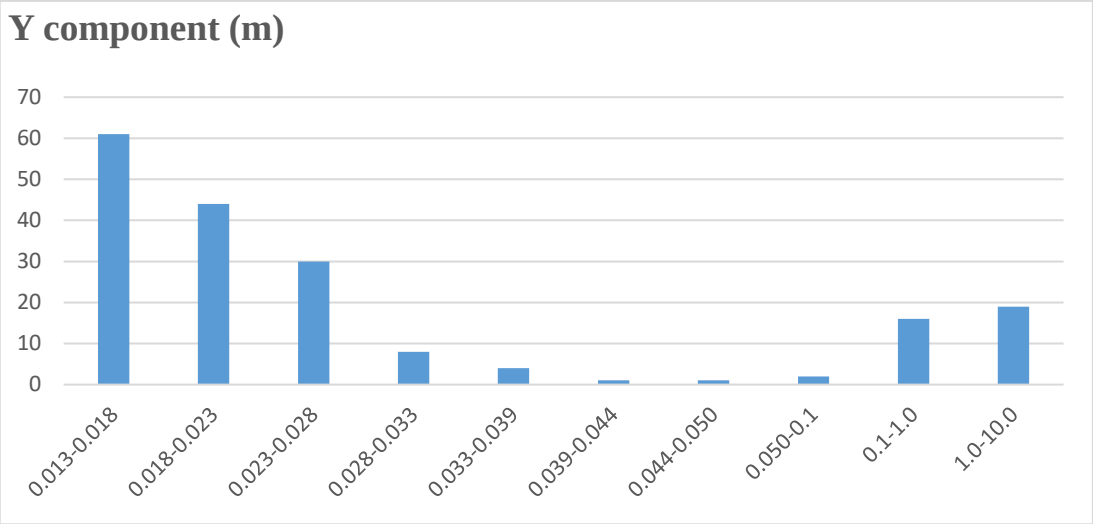

Chart 4-14: Configuration 5 - X component values grouped

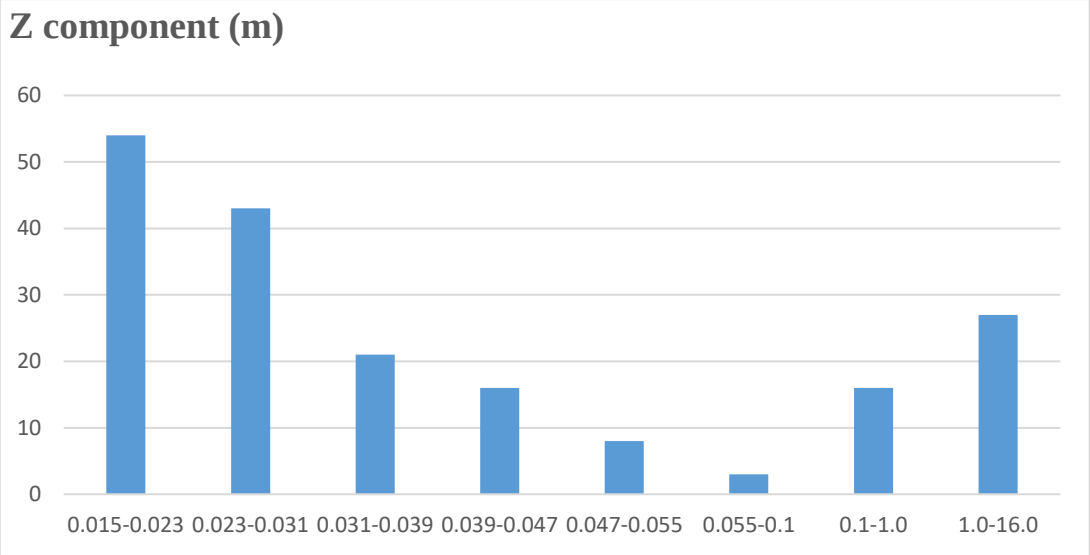

Chart 4-15: Configuration 5 - Z component values grouped

In the fifth configuration, the tendency of the first two configurations is observed, where moving from highest accuracies to lower ones the number of cells decreases. The first class range is the most dense with the highest number of cells in it. Values higher than 1 m should be considered as outliers.

The following table shows estimated precision per each marker distributed across the survey area.

Marker	GCP/CP	X (mm)	Y (mm)	Z (mm)
1	1	19	19	23
2	0	19	19	19
3	1	19	19	22
4	0	16	16	22
5	0	16	16	17
6	0	NaN	NaN	NaN
7	0	NaN	NaN	NaN
8	1	13	13	15
9	0	NaN	NaN	NaN
10	0	14	14	22
11	0	14	14	18
12	0	NaN	NaN	NaN
13	0	16	16	24
14	0	16	16	18
15	0	17	17	22
16	1	20	20	27
17	0	19	19	20
18	1	21	21	28
19	0	14	14	18
20	0	14	14	15
Total GCPs error		18	18	23
Total CP error		16	16	20

Table 4-9: Configuration 5 - Estimated precision of each marker

In the table above, the values of 1 and 0 in the second column are related to the GCPs and Check Points, respectively.
Following the results estimated by U.Ph.O., it can be observed that average accuracy along X-axis, Y-axis, and Z-axis are 18 mm, 18 mm, and 23 mm respectively, while Check Points have errors of 16 mm, 16 mm, and 20 mm along X,Y, and Z axis respectively.
Following table shows simulation results obtained by Agisoft Metashape Pro, where the signed values are coherent with direction of positive axis.

Marker	GCP/CP	X (m)	Y (m)	Z (m)	X error (mm)	Y error (mm)	Z error (mm)
7	0	400097.3	4000110	300.66	-1	0	15
6	0	400105.5	4000119	300.713	2	1	16
8	1	400103.5	4000105	300.052	9	1	2
5	0	400113.4	4000114	300.371	5	-9	-12

Marker	GCP/CP	X (m)	Y (m)	Z (m)	X error (mm)	Y error (mm)	Z error (mm)
20	0	400109.8	4000106	300.125	24	3	13
4	0	400120.5	4000108	299.953	14	-5	-10
9	0	400112.8	4000098	299.691	16	-4	18
1	1	400113.2	4000130	300.947	-9	-5	-12
2	0	400121.2	4000123	300.353	3	-1	-32
3	1	400127.4	4000118	300.12	-1	-7	11
12	0	400087.3	4000101	300.545	10	9	36
11	0	400095.7	4000094	300.062	2	3	25
10	0	400104.4	4000087	299.49	15	7	64
19	0	400092.5	4000091	299.769	12	6	13
13	0	400079.1	4000091	300.528	-3	16	13
18	1	400069.3	4000084	300.937	-25	14	10
14	0	400087.5	4000084	299.891	10	9	1
17	0	400080.1	4000076	299.792	8	4	0
15	0	400096	4000076	299.423	34	1	-19
16	1	400087.5	4000069	299.417	26	-4	-11
Total GCP error					17	8	10
Total CP error					14	7	25

Table 4-10: Configuration 5 - Empirical precision of each marker

Analysis

The results of expected precision obtained by U.Ph.O. and those obtained from the survey are compared and some conclusion is made below.

To begin with, it has to be noted that GCPs were not truly placed evenly across the survey area. What is more, the markers were located closer to the center of the area due to the presence of high trees along borders of the survey area, which led to unavailability of getting data from certain portions of area. Also, using the DSM of higher resolution would possibly have better results after processing data with U.Ph.O. tool.

For the visualization purposes, the comparison of GCP accuracy results obtained from U.Ph.O. (Estimated) and from the real case study (Empirical) are shown in the charts below.

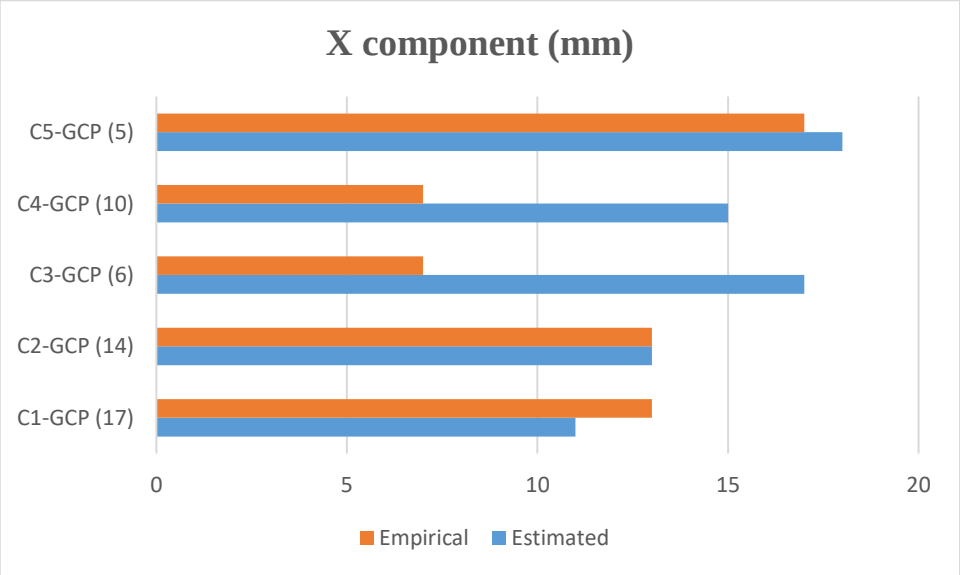

Chart 4-16: GCP X component values compared

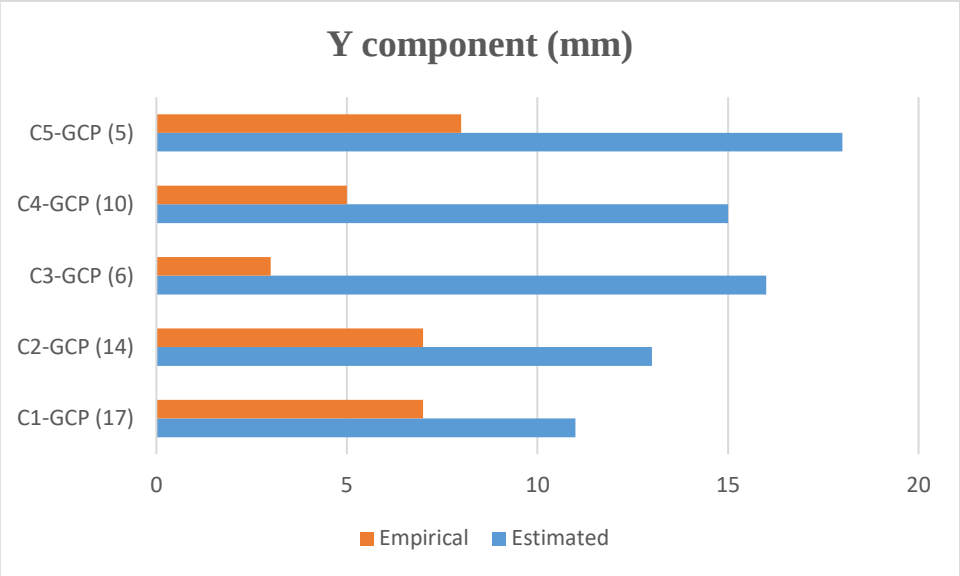

Chart 4-17: GCP Y component values compared

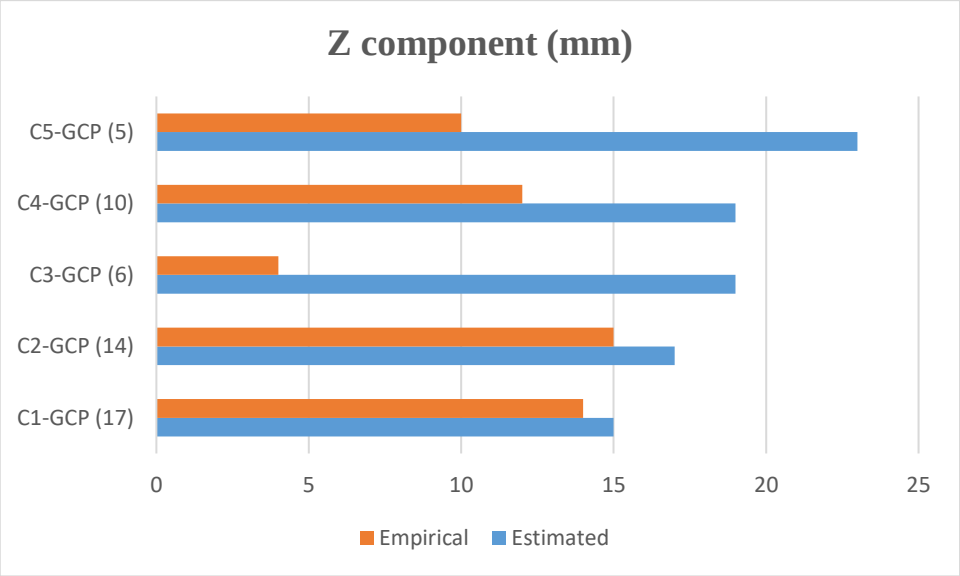

Chart 4-18: GCP Z component values compared

As well as planimetric components, altimetric one shows the expected precision up to two centimeters. But it also can be seen that almost every estimated value in each case is higher than that obtained from real case study. The estimated precision values improve with the increasing of GCP number, as it was expected. Even though it can be seen in the third configuration that the accuracy values are good, it should in general be avoided, because the configuration is not fixed and the least square adjustment is not able to check a representative value of the accuracy.

Summing up GCP RMSE results, it has to be mentioned that the best combination between accuracy and GCP distribution was demonstrated by the first configuration.

CONCLUSION

The advances in technologies these days made UAV become widely used instrument in many applications. UAV, when equipped with a digital camera, has a lot to offer in scientific research, giving opportunity to use it in a photogrammetric survey for the image acquisition. This makes it possible to conduct less dangerous survey in short period of time meeting accuracy requirements. Yet, it is affected by several factors such as environmental condition, battery life, sensor quality, payload, etc.

The resultant map from a photogrammetric processing comes with distortions and other imperfections that can be improved till some point. One of the most important improvements can be made by understanding how the number and distribution of GCPs affect the accuracy of photogrammetric model.

This project aimed to find out the best configuration in order to create good quality map. The flight planning tool, the U.Ph.O., helped to make a prediction on the accuracy before conducting the flight for the reason of getting higher accuracy results. This tool uses rigorous method of network simulation giving image overlapping and expected precision information for planimetric components X,Y, and for altimetric component Z.

The case study was conducted with a single flight at the altitude of 30 meters in the area outside the Praglia village (Genoa, Region Liguria). In order to understand the accuracy fluctuations depending on the number and distribution of GCPs, the project was decided to be performed in five scenarios with twenty markers available:

- Configuration 1:

where 17 markers served as GCPs evenly distributed across the area and other 3 served as check points. Following the results estimated by U.Ph.O., the average GCP accuracy along X-axis, Y-axis, and Z-axis are 11 mm, 11mm, and 15 mm respectively, while Check Points have errors of 10 mm, 10 mm, and 11 mm along X,Y, and Z axis respectively. And following the results obtained from Agisoft Metashape Pro, the average GCP accuracy along X-axis, Y-axis, and Z-axis are 13 mm, 7 mm, and 14 mm respectively, while Check Points have errors of 2 mm, 8 mm, and 20 mm along X,Y, and Z axis respectively.

- Configuration 2:

where 14 markers that are placed along the borders of the study area were chosen to serve as GCPs, and other 6 as check points. Following the results estimated by U.Ph.O., the average GCP accuracy along X-axis, Y-axis, and Z-axis are 13 mm, 13 mm, and 17 mm respectively, while Check Points have errors of 10 mm, 10 mm, and 13 mm along X,Y, and Z axis respectively. And following the results obtained from Agisoft Metashape Pro, the average GCP accuracy along X-axis, Y-axis, and Z-axis are 13 mm, 7 mm, and 15 mm respectively, while Check Points have errors of 8 mm, 6 mm, and 18 mm along X,Y, and Z axis respectively.

- Configuration 3:

where opposite to the second configuration, the GCPs were chosen to be those in the center of the area, and others served as check points. Following the results estimated by U.Ph.O., the average GCP accuracy along X-axis, Y-axis, and Z-axis are 17 mm, 16 mm, and 19 mm respectively, while Check Points have errors of 27 mm, 27 mm, and 80 mm along X,Y, and Z axis respectively. And following the results obtained from Agisoft Metashape Pro, the average GCP accuracy along X-axis, Y-axis, and Z-axis are 7 mm, 3 mm, and 4 mm respectively, while Check Points have errors of 17 mm, 7 mm, and 60 mm along X,Y, and Z axis respectively.

- Configuration 4:

where markers from equal one half were chosen to serve as GCPs, and the other half as check points. Following the results estimated by U.Ph.O., the average GCP accuracy along X-axis, Y-axis, and Z-axis are 15 mm, 15 mm, and 19 mm respectively, while Check Points have errors of 46 mm, 46 mm, and 58 mm along X,Y, and Z axis respectively. And following the results obtained from Agisoft Metashape Pro, the average GCP accuracy along X-axis, Y-axis, and Z-axis are 7 mm, 5 mm, and 12 mm respectively, while Check Points have errors of 20 mm, 17 mm, and 196 mm along X,Y, and Z axis respectively.

- Configuration 5:

where four markers from each end and one in the center served to be GCPs, while the rest of the markers were chosen serve as check points. Following the results estimated by U.Ph.O., the average GCP accuracy along X-axis, Y-axis, and Z-axis are 18 mm, 18 mm, and 23 mm respectively, while Check Points have errors of 16 mm, 16 mm, and 20 mm along X,Y, and Z axis respectively. And following the results obtained from Agisoft Metashape Pro, the average GCP accuracy along X-axis, Y-axis, and Z-axis are 17 mm, 8 mm, and 10 mm respectively, while Check Points have errors of 14 mm, 7 mm, and 25 mm along X,Y, and Z axis respectively.

After having performed flight planning with U.Ph.O. tool, the flight itself has taken place. All the 87 images acquired, were then used in the Agisoft Metashape Pro software to process the data to be compared with expected precision values afterwards.

Summing up the whole project, it has to be said that the first and the fifth configurations demonstrated the most accurate results. The first configuration shows an accuracy of both GCPs and check points up to 1 cm across all the area, while the fifth one showed a bit higher error. For the other configurations, the obtained results underlined lower or inhomogeneity accuracy values for the check points. In configurations 1 and 5 the results are homogeneous due to the homogeneous distribution of GCPs. In effect, the configuration 5 have only 5 GCPs while the Configuration 1 have 17 GCPs. The use of U.Ph.O. permit to evaluate realistically the expected error of the survey with a good agreement with the empirical results obtained in the present thesis work.

BIBLIOGRAPHY

[1] Sanz-Ablanedo, E., Chandler, J., Rodríguez-Pérez, J., & Ordóñez, C. (2018). Accuracy of Unmanned Aerial Vehicle (UAV) and SfM Photogrammetry Survey as a Function of the Number and Location of Ground Control Points Used. *Remote Sensing*, *10*(10). https://doi.org/10.3390/rs10101606

[2] Oniga, V. E., Breaban, A. I., Pfeifer, N., & Chirila, C. (2020). Determining the Suitable Number of Ground Control Points for UAS Images Georeferencing by Varying Number and Spatial Distribution. *Remote Sensing*, *12*(5). https://doi.org/10.3390/rs12050876

[3] Cabo, C., Sanz-Ablanedo, E., Roca-Pardinas, J., & Ordonez, C. (2021). Influence of the Number and Spatial Distribution of Ground Control Points in the Accuracy of UAV-SfM DEMs: An Approach Based on Generalized Additive Models. *IEEE Transactions on Geoscience and Remote Sensing*, *59*(12). https://doi.org/10.1109/tgrs.2021.3050693

[4] Passoni, D. (2019, September). *Innovative Tools For Planning, Analysis, and Management of UAV Photogrammetric Surveys*. University of Genoa.

[5] Nagendran, S. K., Tung, W. Y., & Mohamad Ismail, M. A. (2018). Accuracy assessment on low altitude UAV-borne photogrammetry outputs influenced by ground control point at different altitude. *IOP Conference Series: Earth and Environmental Science*, *169*. https://doi.org/10.1088/1755-1315/169/1/012031

[6] Tahar, K. N. (2013). AN EVALUATION ON DIFFERENT NUMBER OF GROUND CONTROL POINTS IN UNMANNED AERIAL VEHICLE PHOTOGRAMMETRIC BLOCK. *The International Archives of the Photogrammetry, Remote Sensing and Spatial Information Sciences*, *XL-2/W2*. https://doi.org/10.5194/isprsarchives-xl-2-w2-93-2013

[7] Gomes Pessoa, G., Caceres Carrilho, A., Takahashi Miyoshi, G., Amorim, A., & Galo, M. (2020). Assessment of UAV-based digital surface model and the effects of quantity and distribution of ground control points. *International Journal of Remote Sensing*, *42*(1). https://doi.org/10.1080/01431161.2020.1800122

[8] Garcia, M. V. Y., & Oliveira, H. C. (2020). The Influence of Ground Control Points Configuration and Camera Calibration for DTM and Orthomosaic Generation using Imagery Obtained from a Low-Cost UAV. *ISPRS Annals of the Photogrammetry, Remote Sensing and Spatial Information Sciences*, *V–1*. https://doi.org/10.5194/isprs-annals-v-1-2020-239-2020

[9] Iheaturu, C. J., Ayodele, E. G., & Okolie, C. J. (2020). An Assessment of the Accuracy of Structure-from-Motion (SFM) Photogrammetry for 3D Terrain Mapping. *Geomatics, Landmanagement and Landscape*, *2*. https://doi.org/10.15576/gll/2020.2.65

[10] Hugenholtz, C., Brown, O., Walker, J., Barchyn, T., Nesbit, P., Kucharczyk, M., & Myshak, S. (2016). Spatial Accuracy of UAV-Derived Orthoimagery and Topography: Comparing Photogrammetric Models Processed with Direct Geo-Referencing and Ground Control Points. *GEOMATICA*, *70*(1). https://doi.org/10.5623/cig2016-102

[11] Agüera-Vega, F., Carvajal-Ramírez, F., & Martínez-Carricondo, P. (2017). Assessment of photogrammetric mapping accuracy based on variation ground control points number using unmanned aerial vehicle. *Measurement*, *98*. https://doi.org/10.1016/j.measurement.2016.12.002

[12] Jaud, M., Passot, S., le Bivic, R., Delacourt, C., Grandjean, P., & le Dantec, N. (2016). Assessing the Accuracy of High-Resolution Digital Surface Models Computed by PhotoScan® and MicMac® in Sub-Optimal Survey Conditions. *Remote Sensing*, *8*(6). https://doi.org/10.3390/rs8060465

[13] Elkhrachy, I. (2021). Accuracy Assessment of Low-Cost Unmanned Aerial Vehicle (UAV) Photogrammetry. *Alexandria Engineering Journal*, *60*(6). https://doi.org/10.1016/j.aej.2021.04.011

[14] Hruska, J., Padua, L., Adao, T., Peres, E., Martinho, J., & Sousa, J. J. (2020). Target Influence on Ground Control Points (GCPs) Identification in Aerial Images. *IGARSS 2020 - 2020 IEEE International Geoscience and Remote Sensing Symposium*. https://doi.org/10.1109/igarss39084.2020.9324222

[15] Garcia, M. V. Y., & Oliveira, H. C. D. (2021). The Influence of Flight Configuration, Camera Calibration, and Ground Control Points for Digital Terrain Model and Orthomosaic Generation Using Unmanned Aerial Vehicles Imagery. *Boletim de Ciências Geodésicas*, *27*(2). https://doi.org/10.1590/s1982-21702021000200015

[16] Ferrer-González, E., Agüera-Vega, F., Carvajal-Ramírez, F., & Martínez-Carricondo, P. (2020). UAV Photogrammetry Accuracy Assessment for Corridor Mapping Based on the Number and Distribution of Ground Control Points. *Remote Sensing*, *12*(15). https://doi.org/10.3390/rs12152447

[17] Kraus, K., Harley, I. A., & Kyle, S. (2011). *Photogrammetry*. De Gruyter.

[18] Weng, Q. (2012). *An Introduction to Contemporary Remote Sensing* (1st ed.). McGraw Hill.

[19] Valavanis, K. P., & Vachtsevanos, G. J. (2015). *Handbook of Unmanned Aerial Vehicles*. Springer Publishing.

[20] Apogeeweb. (2018, October 19). *How the Drone Works: Principle and Core System*. https://www.apogeeweb.net/article/131.html#:%7E:text=What%20is%20the%20working%20principle,the%20lift%2C%20and%20vice%20versa.

[21] CFD Flow Engineering. (2021, December 17). *Working Principle and Components of Drone ·*. https://cfdflowengineering.com/working-principle-and-components-of-drone/

[22] *Understand How Drones Work - Fast Guide*. (2021, April 21). Comedronewithme. https://comedronewithme.com/how-drones-work/

[23] Murison, M. (n.d.). *Fixed-Wing vs Multirotor: Which Drone Should You Choose for Aerial Surveying?* Dji.Com. https://enterprise-insights.dji.com/blog/fixed-wing-vs-multirotor-drone-surveying

[24] Giordan, D., Adams, M. S., Aicardi, I., Alicandro, M., Allasia, P., Baldo, M., de Berardinis, P., Dominici, D., Godone, D., Hobbs, P., Lechner, V., Niedzielski, T., Piras, M., Rotilio, M., Salvini, R., Segor, V., Sotier, B., & Troilo, F. (2020). The use of unmanned aerial vehicles (UAVs) for engineering geology applications. *Bulletin of Engineering Geology and the Environment*, *79*(7), 3437–3481. https://doi.org/10.1007/s10064-020-01766-2

[25] EASA. (2021, September 30). *Easy Access Rules for Unmanned Aircraft Systems (Regulation (EU) 2019/947 and Regulation (EU) 2019/945)*. https://www.easa.europa.eu/document-library/easy-access-rules/easy-access-rules-unmanned-aircraft-systems-regulation-eu

[26] Lillesand, T. (2015). *Remote Sensing and Image Interpretation* (7th ed.). Wiley.

[27] Egels, Y. (2001). *Digital Photogrammetry*. Amsterdam University Press.

[28] Et.Al, E. M. M. (2022). *Introduction to Modern Photogrammetry* (1st ed.). WILEY INDIA.

[29] Konecny, G. (2014). *Geoinformation: Remote Sensing, Photogrammetry and Geographic Information Systems, Second Edition* (2nd ed.). CRC Press.

[30] Morgan, J. L., Gergel, S. E., & Coops, N. C. (2010). Aerial Photography: A Rapidly Evolving Tool for Ecological Management. *BioScience*, *60*(1), 47–59. https://doi.org/10.1525/bio.2010.60.1.9

[31] Agisoft LLC. (2021). *User Manuals*. Agisoft Metashape Pro. https://www.agisoft.com/downloads/user-manuals/

[32] Jeziorska, J. (2020, May). *Mapping and Analysis using UAS*. Ncsu-Geoforall-Lab.Github.Io. https://ncsu-geoforall-lab.github.io/uav-lidar-analytics-course/